ELSEVIER

Journal of Nuclear Materials 312 (2003) 21–49

journal of nuclear materials

www.elsevier.com/locate/jnucmat

Thermodynamics of the O–U system. I – Oxygen chemical potential critical assessment in the UO_2–U_3O_8 composition range

D. Labroche [a], O. Dugne [a], C. Chatillon [b,*]

[a] *Commissariat à l'Energie Atomique VALRHO, DTE/STME, BP. 111, 26702 Pierrelatte, France*

[b] *Laboratoire de Thermodynamique et Physico-Chimie Métallurgiques (UMR 5614 CNRS/UJF/INPG)-ENSEEG, BP. 75, 38402 Saint Martin d'Hères, France*

Received 10 September 2001; accepted 14 October 2002

Abstract

A critical assessment of oxygen chemical potential of UO_{2+x}, U_4O_9 and U_3O_8 oxide non-stoichiometric phases as well as of diphasic related domains has been performed in order to build up primary input data files used in a further optimization procedure of thermodynamic and phase diagram data for the uranium–oxygen system in the UO_2–UO_3 composition range. Owing to the fact that original data are very numerous, more than 500 publications, a twofold process is used for the assessment – (i) first a critical selection of data is performed for each method of measurement together with a careful estimate of their uncertainties, (ii) second a reduction of the total number of data on the basis of a chart with fixed intervals of temperature and composition that allows a comparison to be made of the results from the various experiments. Results are presented for chemical potentials of oxygen with their associated uncertainties.

1. Introduction

The uranium–oxygen system has been mainly studied during the 1960s, in the context of increasing nuclear energy requirements, in order to understand and anticipate the behavior of urania fuel and its interactions with cladding, the confinement gas and coolant. The great amount of data from some 500 publications, requires a careful selection before any mathematical correlation between phase diagram and thermodynamic data in order to describe the binary U–O system is undertaken. Non-stoichiometric and liquid phases will be considered in this assessment.

Owing to this large set of original experimental data, and to the complexity of this system – at least four main compounds exist, UO_2, U_4O_9, U_3O_8 and UO_3 – different phase diagrams have been proposed together with data selections [1–4]. Only one optimisation study was performed using thermodynamic data in conjunction with phase diagram data using a generalized Gauss–Newton method [5]. Taking account of the non-stoichiometric domains remains very important for the description of the $UO_{2\pm x}$ phase [5] since this domain plays an important role at high temperatures, but also for the two other U_4O_{9-y} and U_3O_{8-z} phases.

For our purpose the use of the Parrot optimizer of Thermocalc software [6] – needs a carefull pre-selection of experimental data with a sound analysis of the causes of errors, followed by an estimate of the uncertainty ranges for each measured quantity. The inverse of the uncertainty is used as a weighting factor in the generalized least square fit method (Gauss–Newton method) of the optimization software. Moreover, the description of solution phases, liquid and non-stoichiometric, must be based on convenient models. Consequently, the

* Corresponding author.
E-mail address: chatillo@ltpcm.inpg.fr (C. Chatillon).

0022-3115/03/$ - see front matter
PII: S0022-3115(02)01322-3

selection of data will be presented in different sections of this work which consider the following topics:

- data selection of the chemical potential of oxygen in the range UO_2–UO_3 as presented in this paper (paper I),
- stability data, non-stoichiometric composition domains and phase transformations for the higher oxides, leading to their Gibbs energy of formation, which are mainly considered in part II of this study (paper II).

Data concerning lattice defects and structures in order to select a simplified description of such defects for inclusion in the thermodynamic description of non-stoichiometry as well as to clarify the most probable stoichiometric like composition, and phase diagram and thermodynamic data selection for the U–UO_2 composition range up to the liquid phase, will be analyzed in further works.

Use of the Parrot optimization procedure [6] will be carried out phase by phase from the data collection because of the increasing number of parameters in the thermodynamic description of the non-stoichiometric regions. A final description and an analysis of optimized results will be presented. Particular attention has been applied not only to the primary data selection, but also to the estimate of the total uncertainty attributed to each type of data. When the determination of a measured quantity accumulates different kinds of independent uncertainties, in order to avoid the use of too large and insignificant uncertainty ranges, the uncertainty is treated by a law analogous to the law of propagation of errors [7] applied independently to each variable:

$$\delta E(\text{total}) = \sqrt{\sum_i (\delta E_i)^2}. \quad (1)$$

This relation implies that these independent uncertainties δE_i show a large probability to compensate each other. As an example, when evaluating the uncertainty for compositions, each δE_i may be uncertainties of the authors (very often published as reproducibility), readers (if published as graphs) and from the reference. However, in some cases, where the result was evidently and unrealistically too small, we used a simple summation – a classical error calculation issued from derivatives. This usual mathematical treatment corresponds in fact to a small number of uncertainty independent causes (usually two) for which compensation effects do not statistically operate (probability < 0.5). Finally, according to the availability of the published experimental details as well as to the authors' discussion, we alternately have either (i) chosen their proposed uncertainty values, (ii) reevaluated them, or (iii) estimated them from analogous experiments.

2. Composition and temperature uncertainty analysis

The knowledge of the composition, often presented as O/U ratios, is important mainly because the stoichiometric domains may be very small and the evolution of the measured quantity may be extremely rapid.

2.1. Compositions and associated uncertainties

Table 1 presents earlier studies dealing with the performance of different techniques used to measure O/U ratios. Easy to run, accurate and not expensive, the gravimetric or thermogravimetric method was very often used. In the estimate of total uncertainties, three cases are encountered:

- cited uncertainties are kept as published,
- those not cited are taken as in Table 1,

Table 1
Summary of the different techniques used to determine the composition O/U ratio of uranium oxides in the UO_{2+x}–U_3O_8 range

Technique	Principle	Uncertainty on O/U ratios	Observations
Polarography	Electrochemical study with mercury droplet [8]	±0.005 [9]	For $O/U > 2.1$
Coulometry	Titration(?) of an intermediate ionic species(?) by oxidation or reduction [8]	±0.003 [9]	Better than polarography for $O/U > 2.01$
Cerimetry titration	Titration of U^{4+} ions by Ce^{4+}, and then titration of excess Ce^{4+} ions	±0.003 [10]	For $2.02 < O/U < 2.667$
Gravimetry and thermogravimetry	Weight loss or weight gain under a controlled atmosphere	±0.003 [11]	This method is re-analyzed in this work
Melting in an inert gas	Melting of the sample in a graphite crucible and analysis of CO_2 quantity	±0.006 [12]	All oxygen is assumed to produce CO_2 No formation of U–O–C compounds
H_2 reduction	Dry H_2 at $T > 1173$ K gives $UO_{2.00}$	±0.002 [13]	Check H_2 for H_2O and O_2 impurities to be <1 ppm (see text part 2.3)

- analytical method not quoted, we arbitrarily chose $\delta x\pm = 0.01$, (x being related to the UO_{2+X} compound).

2.2. The U_3O_8 oxidized composition reference for gravimetry or thermogravimetry

This technique is based on the calcination reaction,

$$UO_{2\pm x} + (6 \pm x)/2O_2 \Longleftrightarrow U_3O_8. \quad (2)$$

It was assumed generally that this reaction at 850 °C in air led to the stoichiometric compound U_3O_8. Some authors used higher temperatures. Conversely, reduction of UO_{2+x} by H_2 was also used, leading to the final product $UO_{2.0\pm0.002}$ [13].

Experimental studies were performed in order to check the U_3O_8 stoichiometric composition after calcination, as presented in Table 2. Differences in results between authors are due to atmospheric compositions, air or $Ar + O_2$ (always 1 atm, 0.21 atm O_2) and to cooling effects. Figs. 1 and 2 show the results, from which we observe a large scatter for atmospheric compositions ($N_2 + O_2$ or dry air). In order to discard a possible influence of N_2, Ackermann and Chang [19] used $Ar + O_2$ mixtures, as well as two techniques in the measurements of O/U ratios (in parallel). Their results show that the O/U ratio never exceeds 2.667 ($= U_3O_8$), and we shall confirm this in the further analysis of oxygen chemical potentials. They observed also that increasing the temperature at constant oxygen (0.21 atm) pressure allowed U_3O_8 to become non-stoichiometric (U_3O_{8-z}). The maximum temperature for stoichiometry at 0.21 atm of O_2 is determined to be 873 K, in agreement with Cordfunke and Aling [16] and Rodriguez et al. [18].

The scatter of results (Figs. 1 and 2) seems to indicate that the N_2 molecule is not inert, not only because some solubility may exist in U_4O_9 and U_3O_8 as already occurs for UO_2 [22], but also because the role of N_2 may be different in different steps of the thermal history of the samples. As an example, the original samples that have been heat treated under air (before the measurements), may have trapped nitrogen, and these sites may not be or partly not be recovered during the measurements. This feature would explain the results of Srirama Murti et al. [21], Fujino et al. [20] and Gerdanian and Dodé [17] obtained by air oxidation in situ, since their compositions are shifted towards U when compared to the values of Ackermann and Chang (Figs. 1 and 2) [19].

As shown by Ackermann and Chang, earlier calcinations at $T > 873$ K may be in error with the assumption that U_3O_8 was stoichiometric. Indeed, Gerdanian and Dodé [17] showed that when cooling slowly in a thermobalance, the sample continues to incorporate oxygen and becomes stoichiometric – the reference at that time being $UO_{2.0}$. Srirama Murti et al. [21] in a temperature cycling experiment with continuous comparison of the same sample cooled in flowing air or in Ar the thermobalance. Gerdanian and Dodé showed also that starting the calcinations from U or UO_2 samples do not lead to the apparently same product, confirming the non evaluated impact of N_2 in the history of the sample under air.

Results of Srirama Murti et al. appear always richer in oxygen at low temperature – the O/U ratio being analyzed by cerimetry – even when taking into account the cerimetric uncertainty range (Table 1). The general trend of these measurements agrees with the non-stoichiometric behaviour above 873 K in air, and we believe the cerimetric titration is probably erroneous by an excess. Schaeffer and Hibbits [13] proved by cross-checking different methods that $U_3O_{8\pm0.01}$ (or $O/U = 2.667 \pm 0.003$) is the upper oxygen content of this compound.

2.3. Rules for composition and uncertainty analysis

As a conclusion for thermogravimetric analysis of composition ratios, we adopted the following rules:

- For in situ thermogravimetry, i.e. analysis of weight gain along a high temperature plateau: U_3O_8 is considered stoichiometric for $T \leqslant 873$ K and $p_{O_2} = 0.21$ atm according to Ackermann and Chang [19]. For other and higher oxidation temperatures, the true final composition of the U_3O_{8-z} oxide is determined by the following relation (least square fit of Ackermann and Chang data):

$$O/U = 1.3752 + 0.0046875T - 6.1855 \times 10^{-6}T^2 + 3.5194 \times 10^{-9}T^3 - 7.3925 \times 10^{-13}T^4, \quad (3)$$

  in the $873 < T < 1500$ K range, and corrections of the authors data have to be made.
- Samples sealed in an ampoule and quenched in water or liquid nitrogen, or cooled rapidly from 1273 K: the above correction with relation (3) is applied, assuming that samples do not readsorb oxygen. However, we cannot determine a cooling speed limit,
- samples analyzed by thermogravimetry (1273–1373 K) or gravimetry ex situ and slowly decreased to room temperature as observed by Gerdanian and Dodé [17]: the stoichiometric U_3O_8 is chosen as a reference for final composition.

The presence of N is considered as equivalent to O in the U_3O_8 final compound whatever is the history of the sample. As a matter of fact, the evaluation of uncertainties as shown in Fig. 1 is clearly different by a factor 10 between air and controlled $Ar + O_2$ atmospheres.

Table 2
Summary of the studies of the U_3O_8 stoichiometric compositions as a function of experimental or preparative conditions

Authors [Ref.]	Initial material	Experimental method	Composition analysis uncertainty	Our conclusion
Lynch et al. [14]	U_3O_8 from calcination at air at 1273 K	Thermogravimetry under air $\delta T = \pm 5$ K	Reference UO_2. U analysis by chemical way $\delta x = \pm 0.01$ (our estimate)	• No quenching, in situ analysis • Application of Ackerman and Chang correction (see text)
Petit and Kienberger [15]	U or UO_3, uranyl fluoride or nitrate	Gravimetry at air $\delta T = \pm 10$ K	• Potentiometry • Reference NBS sample • $\delta x = \pm 0.015$	• U, U peroxide, fluoride oxidation at 1123 K into U_3O_8 • UO_3, Uranyl nitrate: oxidation at 1273 K then maintained at 1123 K
Cordfunke and Aling [16]	γ-UO_3 (by DRX)	O_2 pressure by static method for $3UO_3 = U_3O_8 + 1/2O_2 (\log p_{O_2} = A/T + B)$	• Gravimetry at 850 °C under air	• U_3O_8 stoichiometric at 882 K, $p_{O_2} = 159$ mm Hg
Gerdanian and Dodé [17]	U metal impurities < 173 ppm	Thermogravimetry with correction for buoyancy and impurities $\delta T = \pm 5$ K	• Gravimetry in situ at air • References UO_2 with CO/CO_2 mixtures • Reference U_3O_8 with air • Observation of weight gain during cooling • $\delta x = \pm 0.001$	• U gives $UO_{2.662}$ at 1073 K • UO_2 gives U_3O_8 ($UO_{2.667}$) at 1073 K • Definitions of the UO_2 and U_3O_8 thermogravimetric references
Rodriguez de Sastre et al. [18]	$UO_{2.012}$	Gravimetry in O_2 gas + carrier gas (unknown) $\delta T = \pm 5$ K	• Approximation on the starting composition • $\delta x = \pm 0.001$	• Cooling under air, and then vacuum at room T • $p_{O_2} = 0.21$ atm, U_3O_8 at 873 K for melted UO_2 samples • $p_{O_2} = 0.21$ atm, $UO_{2.675}$ at 1073 K for sintered UO_2 samples
Ackerman and Chang [19]	U or UO_2	Thermogravimetry under $Ar + O_2$ $\delta T = \pm 5$ K	• Analysis at T • Control by melting in an inert gas • $\delta x = \pm 0.002$	• U_3O_8 stoichiometric for $p_{O_2} = 0.21$ atm, at 873K • Composition $U_3O_{8-z} = f(T)$
Fujino et al. [20]	U metal impurities < 40 ppm	Thermogravimetry under air $\delta T = \pm 5$ K	• Gravimetry in situ at $T = 1073$ K • $\delta x = \pm 0.005$	• O/U ratio $= f(T)$
Srirama Murti et al. [21]	UO_2 oxidized at 723 K at air into U_3O_8	Thermogravimetry under air $\delta T = \pm 5$ K	• Reference UO_2 'nuclear grade' • Cooling under air or Ar • U_3O_8 oxidized at air at 1073 K, quenched under air	• U_3O_8 obtained at 873–973 K under air and quenched under Ar. • $\delta x = \pm 0.01$

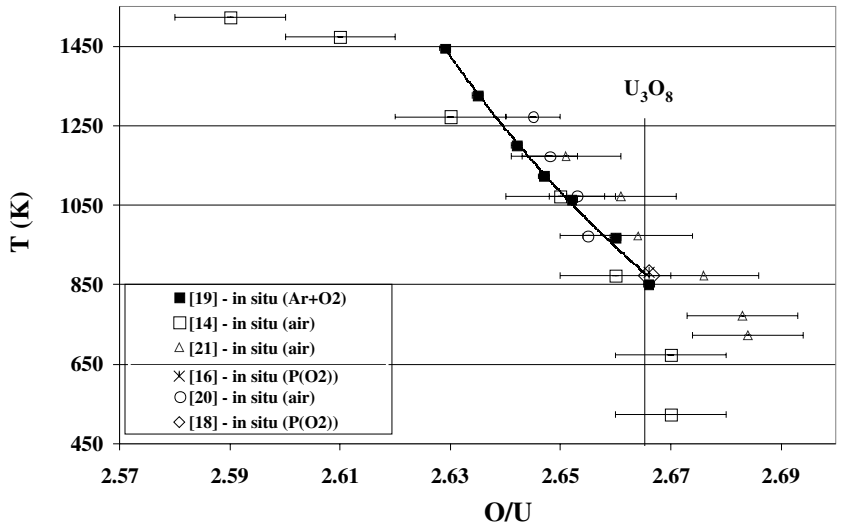

Fig. 1. $U_3O_{8\pm z}$ compositions issued from thermogravimetric studies performed in situ by calcination of U or UO_2 samples under various oxidizing atmospheres with a partial oxygen pressure of 0.21 atm. The mentioned uncertainty bars are in agreement with the estimated ones in this study.

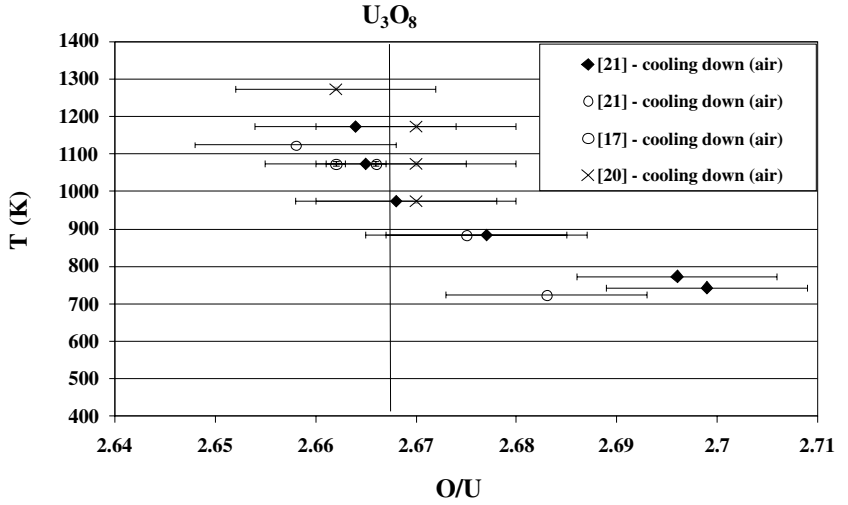

Fig. 2. $U_3O_{8\pm z}$ compositions issued from thermogravimetric studies performed by calcination in air, the O/M ratios been determined after cooling down under the same atmosphere.

2.4. Temperature uncertainties

Temperature in this range (700–1500 K) was always measured by thermocouples, and the authors quoted their reproducibility. So, as a general rule we have chosen an uncertainty $\delta T = \pm 5$ K that takes into account of reproducibility, lack of calibration, ageing, thermal gradients and electrical connections. In case of special mention of a calibration procedure, some authors proposed ± 2 K, which we accept. For X-ray diffraction, as the material analyzed is at the surface of a substrate, the uncertainty is fixed at ± 10 K.

3. Chemical potentials by the e.m.f. method

3.1. Principle of the method and source of uncertainties

Galvanic cells of the following type were used,

$$\mathrm{Pt, Ni, NiO|ZrO_2, 15mol.\%CaO|UO_{2+X}, Pt}$$

Table 3
Summary of e.m.f. studies performed in the UO_2–U_4O_9 composition range

Authors [Ref.]	Sample preparation and nature	Technique Experimental data range	Composition analysis and uncertainty	Atmosphere and conditions of measurements
Kiukkola [24]	• UO_2 oxidized at $t < 200$ °C • $UO_2 + U_3O_8$ mixtures, heat treated at 1000 °C in a sealed ampoule (quartz) • Pellets	• Fe, FeO/ZrO_2, 0.15 CaO/UO_{2+x}, Pt • Reference Fe–FeO Sundman [23] • $2.085 < O/U < 2.247$	• Oxidation in air at 800 °C → (U_3O_8) • $\delta x = \pm 0.01$	• Ar deoxidized by Cu (200 °C) and dehydrated
Aronson and Belle [25]	• $UO_{2.03}$ oxidized at 200 °C or reduced by H_2 at 800 °C, then heat treated in Vycor ampoules • $UO_2 + U_3O_8$ mixtures sealed in quartz, 1000 °C • Pellets	• Fe, FeO/ZrO_2, 0.15CaO/UO_{2+x}, Pt • Reference Fe–FeO Sundman [23] • $2.01 < O/U < 2.2$	• Chemical titration of U^{4+} and total U • $\delta x = \pm 0.05$ • Phase idendification by XRD	• Ar or He dehydrated
Markin and Bones [26]	• No information • Pellets	• Ni, NiO/ZrO_2, 0.15CaO or/ThO_2, 0.075Y_2O_3/UO_{2+x}/Pt • Ref. Charrette (see Appendix A) • $2.012 < O/U < 2.188$	• Melting and reaction with C → CO_2 volumetric method • $\delta x = \pm 0.6\%$ (our estimate)	• Ar deoxidized by Cu/CuO • Dehydrated by Mg perchlorate
Marchidan and Matei [27]	• $UO_{2.04}$ obtained from fuels (high grade) • $UO_{2.11,\ 2.19\ \text{and}\ 2.21}$ from uranyl nitrate • Pellets sintered under N_2 at 1523–1573K	• Fe, FeO/ZrO_2, 0.15CaO/UO_{2+x}, Pt • Ref. Sundman [23] • $2.04 < O/U < 2.21$	• Air oxidation at 1073–1373 K • $\delta x = \pm 0.01$ (our estimate)	• Vacuum as in [31]?
Marchidan and Matei-Tanasescu [28–30]	• No information	• Fe, FeO/ZrO_2, 0.15CaO/UO_{2+x}, Pt • Ref. Sundman [23] • $2.18 < O/U < 2.54$	• Gravimetry as in Ref. [27] • $\delta x = \pm 0.01$ (our estimate)	• Vacuum after [31]
Marchidan and Matei-Tanasescu [31]	• Pellets of UO_{2+x} • Sintered at 1250 K	• Fe, FeO/ZrO_2, 0.15CaO/UO_{2+x}, Pt • Ref. Sundman [23] • $O/U = 2.125, 2.63$	• Gravimetry as in Ref. [27] • $\delta x = \pm 0.01$ (our estimate)	• Vacuum, 10^{-6} Torr
Nakamura and Fujino [32]	• $UO_2(NH_3)_{a2}$, $6H_2O$ oxidized into U_3O_8, in air, 800 °C, then reduction H_2, 1000 °C. Sintered at 1200 °C, vacuum • U oxidized, air, 800 °C then reduction, H_2, 1000 °C	• Ni, NiO/ZrO_2, 0.11CaO/UO_{2+x}, Pt • Ref. Charrette (see Appendix A)	• Coulometry in situ • Ref. $E = 0$ mV at 1000 °C for $x = 0.0088$ • $2.003 < O/U < 2.33$ • $\delta x = \pm 0.004$ for $0.11 < x < 0.15$	• Purified He

Saito [33]	• $UO_{2.09}$ oxidized in air, at 200 °C, time dependent • $UO_{2.09} + UO_2$ mixtures (UO_2 obtained by H_2 reduction at 900 °C) • Pellets	• Ni, NiO/ZrO_2–0.11CaO/UO_{2+x}, Pt • Ref. Charrette (see Appendix A) • $2.04 < O/U < 2.34$	• Gravimetry, air, 800 °C • $\delta x = \pm 0.003$ (our estimate)	• Vacuum and then purified Ar
Martin and Bones [34]	• Two commercial UO_2 sintered samples • Machined thin pellets	• Ni, NiO/ZrO_2 stab/UO_2/Ni • Sealed and pumped vessel		• Special device for low oxygen potential • 1 atm purified Ar
Baranov and Godin [35]	• Sintered and machined thin pellets	• Fe, FeO/ThO_2 alloyed/UO_2, Pt and pumped • Sealed and pumped vessel	• Polarography • $\delta x = \pm 0.005$ (our estimate) • And in situ coulometry • Reference to be corrected	• Ambient p_{O_2} controlled by oxygen pump • Special device for low oxygen potential

the reference electrode being either Ni/NiO or Fe/FeO powder and compacted mixtures. The Gibbs free energy $\Delta_r G$ (at constant total pressure = 1 bar of Ar generally) corresponds to the reaction:

$$2\mathrm{Ni} + 2/y\mathrm{UO}_{2+x+y} \leftrightarrow 2\mathrm{NiO} + 2/y\mathrm{UO}_{2+X} \tag{4}$$

$$\text{and } \Delta_r G = 4EF = \mu_{O_2}(\mathrm{UO}_{2+x}) - \mu_{O_2}(\mathrm{Ni/NiO}). \tag{5}$$

The number 4 accounts for the number of exchanged electrons, F is the faraday constant, E the measured voltage and μ_{O_2} are the chemical potentials of oxygen in UO_{2+X} or for the diphasic Ni/NiO reference mixture. As two references were used, Ni/NiO or Fe/FeO, we first compared these references (see the appendix) in order to select the following Gibbs free energies:

$$\mu_{O_2} = (\mathrm{Fe/FeO}) = -526\,107 + 128.29T \ (210 \pm \mathrm{J\,mol^{-1}}), \tag{6}$$

which is the one retained by Sundman [23] and

$$\mu_{O_2} = (\mathrm{Ni/NiO}) = -467\,302.6 + 169.8T \ (\pm 210 \ \mathrm{J\,mol^{-1}}). \tag{7}$$

The whole set of e.m.f. experimental works in the UO_2–UO_3 composition range is presented in Table 3 and uncertainties in Table 4.

The e.m.f. uncertainties are treated according to the law of propagation of errors [7], that is for the Gibbs free energy of reaction (4) and relation (5):

$$\delta\mu_{O_2} = \sqrt{[2\delta\Delta_r G(\mathrm{ref.})]^2 + [4F\delta E(\mathrm{read.})]^2 + [4F\delta E(\mathrm{meas.})]^2}, \tag{8}$$

ref., read., and meas. account respectively for reference electrode (relations (6) and (7)), for reading from graphs and for statistical fluctuations of measurements (standard deviation) or reproducibility given by the authors.

Such a treatment leads to uncertainties of about 1%, which is really a low value compared to other techniques in thermodynamic determinations. Indeed, this treatment does not take into account the possibility of systematic errors as for example extraneous reactions with the electrolyte, a feature observed by some authors, or modifications of the nature of the electrolyte conductivity with temperature and/or working oxygen potentials as well as oxygen leaks or short circuit. These systematic or erratic errors or trends can be detected only by comparison with other experimental techniques. Firstly, the comparison will be done in a self-consistent way between all the different data obtained from e.m.f. measurements.

Table 4
Uncertainties according either to the propagation law of errors or by simple summation of errors proposed by the authors or estimated by us for the e.m.f. studies

Authors [Ref.]	For $O/U = 2 + x$ $\pm\delta x$	T (K)δT	δE (mV) readings on graph	δE (mV) measurement	$\delta(\Delta G_{Ref.})$ J/mol	$\delta\mu(O_2)$ propagation law J/mol	$\delta\mu(O_2)$ summation J/mol
Kiukkola [24]	0.01	5	0.6	3	210	1253	1810
Aronson and Belle [25]	0.005	5	0.7	3.1 3 for (Fe/FeO/Ni/NiO) (0.1 for readings)	210	1296	1887
Markin and Bones [26]	0.6% According to [9]	5	0	2 (Reproducibility) 3 for (Ni/NiO/Fe/FeO)	210	1975	2350
Marchidan and Matei-Tanasescu [27–31]	0.01	5	0.6	3	210	1253	1810
	Our estimate 0.01	5	0.0 for $UO_{2.125}$ and $UO_{2.63}$	3	210	1232	1578
Nakamura and Fujino [32]	0.004	5	1	3	210	1291	1964
Saito [33]	0.003	5	0.9	2 (Monophasic)	210	945	1540
				4 (Diphasic)		1637	2312
Markin and Bones [34]	0.002	5	0	2	210	800	982
Baranov and Godin [35]	0.005	15	5	2	210	2090	2912

3.2. Selection of a consistent e.m.f. data set

The direct comparison of e.m.f. raw data is not possible since each set is dependent on three variables, composition, temperature and oxygen potentials, the probability of overlap being very low. However, the inclusion of all these raw data directly into an optimization procedure can render the calculations non-convergent. Moreover, as the e.m.f. data are largely more numerous than other data, the optimized results could be over emphasized by their total weight. However, in the Parrot optimizer a supplementary weight in addition to the uncertainty may be managed independently for each set of data or for any experiment to counterbalance this effect.

In order to circumvent these difficulties, we prefer to treat the e.m.f. data sets altogether in a consistent manner when building a chart with regular composition and temperature steps. The temperature step is chosen as 100 K, meanwhile the composition one is chosen as $\delta(O/U) = 0.01$.

Among the e.m.f. works, those of Markin and Bones [34] and Baranov and Godin [35] were for compositions very close to $UO_{2.0}$ (1.999–2.004) and we cannot treat their results with the same chart as others because there is practically no overlap and the variations close to UO_2 become very large and not, a priori, qualitatively known. Markin and Bones [34] compared the form of the merging of their experimental with earlier data [26] at $O/U \approx 2.01$. Their conclusion was that below 2.01 or 2.02 – (i) the oxygen potential is very low, and (ii) UO_{2+x} reacted with the electrolyte. Consequently the usual technique must be improved. In the present work, we do not discuss the measurements close to UO_2, and the two studies above [34,35] will be discussed in another paper which deals with the UO_{2-x} composition range, and our chart applies to $O/U = 2.01$ up to the phase limit rich in oxygen.

3.2.1. Phase limit from e.m.f. measurements

The application of the chart requires quite regular or a known evolution of the measured quantity, i.e. the e.m.f. voltage, with the two variables x (or O/U ratio) and T, discarding any discontinuity as occurs at the phase limit. Thus, we first analyse the e.m.f. evolution in

order to determine the phase limit and consequently retain the data corresponding to the monophasic domain UO_{2+x}. An example of phase limit observation by e.m.f. is shown in Fig. 3, and the set of data obtained is compared with all the available literature data in Fig. 4. The uncertainty associated with limits deduced from graphs as Fig. 3 accounts for ±12.5 K, and the total uncertainty must take into account an uncertainty of ±5 K for thermocouple measurements, and so:

$$\delta T(\text{phase limit deduced in this work}) = +\sqrt{12.5^2 + 5^2} = \pm 13.5 \text{ K}. \quad (9)$$

3.2.2. Chart for comparison of e.m.f. data

The following treatments by least square fits were used only for building the chart nodes that are significant for each data set – that is within the O/U or T range of each author-the aim being to redistribute each data

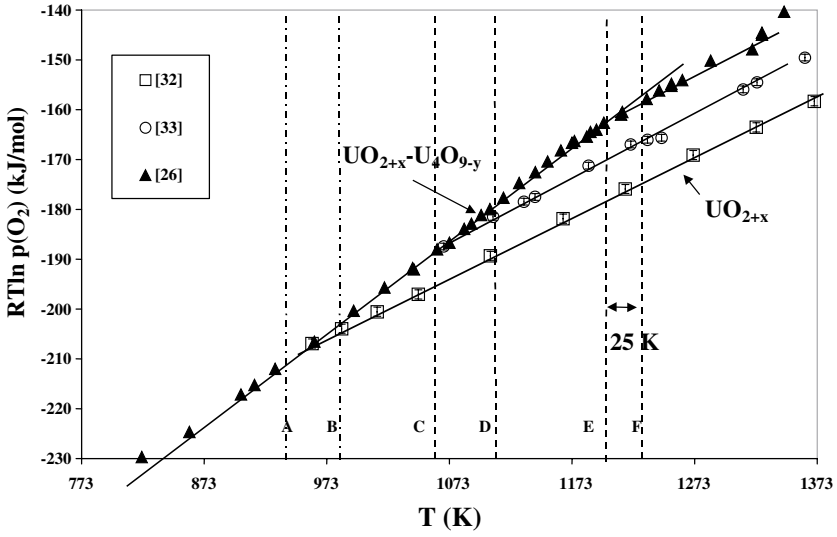

Fig. 3. Evolution of the molar partial Gibbs enthalpy of O_2 versus temperature for different O/U ratios and example of transitions between the UO_{2+x} monophasic domain and the UO_{2+x}–U_4O_9 diphasic region for three O/U ratios. The transition temperature limits are represented by the A–B, C–D and E–F points for the three O/U.

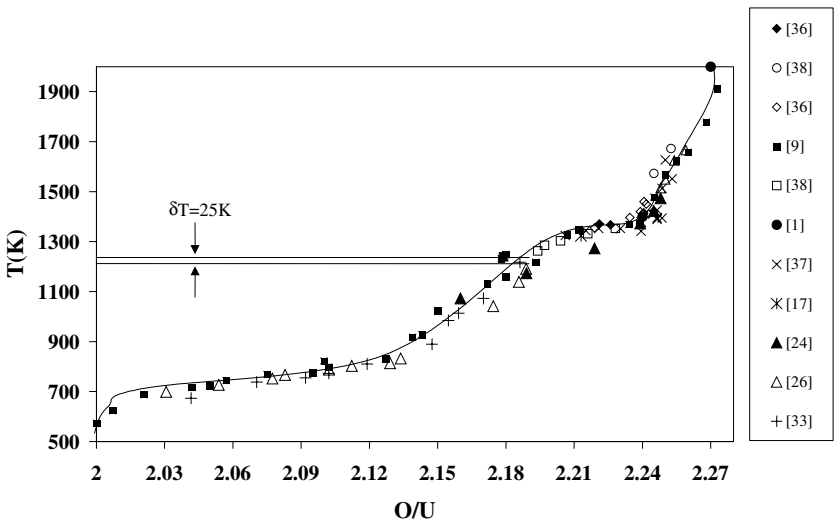

Fig. 4. The set of experimental determinations of the upper phase boundary of the UO_{2+x} domain used to select data in the different monophasic UO_{2+x} and diphasic UO_{2+x}–U_4O_9 domains.

set along chart intervals. These least square fits were never used as intermediate statistical treatments of errors in order to keep original uncertainties that will be used further in the optimization procedure as weights for the raw data redistributed on the chart.

Firstly, the isoconcentration measurements are by the method of least squares fitted versus the inverse of temperature, as shown in Fig. 5. Secondly, the evolution of these potentials at constant temperature and for 100 K intervals are then fitted for the same author (Fig. 6) as a function of composition, and a set of values is stored in a chart (x, T) with increments, $\delta x = 0.01$, $\delta T = 100$ K.

3.2.3. Comparison of different data sets

The comparison takes into account two criteria:

- The trend must agree with usual trends of thermodynamic laws.
- The difference between sets of data must not exceed their total allocated uncertainty.

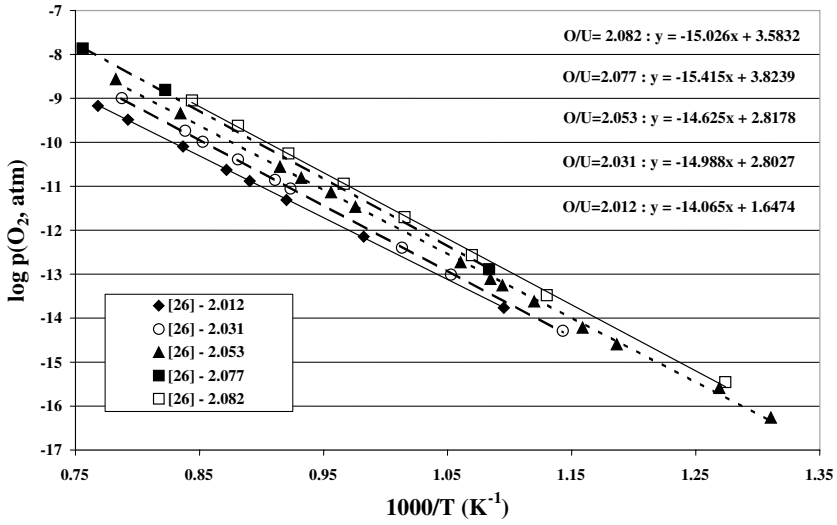

Fig. 5. Evolution of the decimal logarithm of oxygen pressures versus the inverse of temperature for different O/U ratios, according to Markin and Bones [26] experimental data.

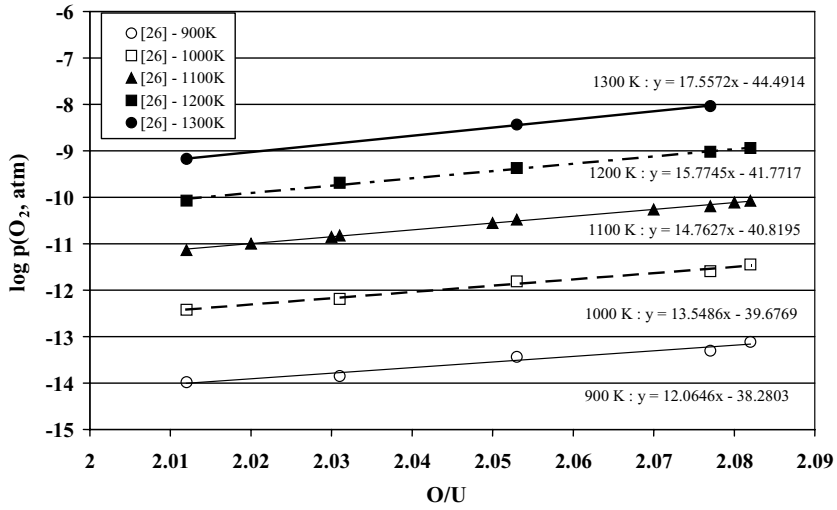

Fig. 6. Least square fits of the decimal logarithm of the isothermal oxygen partial pressure versus composition ($x = O/U$), based on Markin and Bones's work [26]. The data presented here are those obtained from a first fit (Fig. 5) in order to select values corresponding to the O/U intervals of our chart.

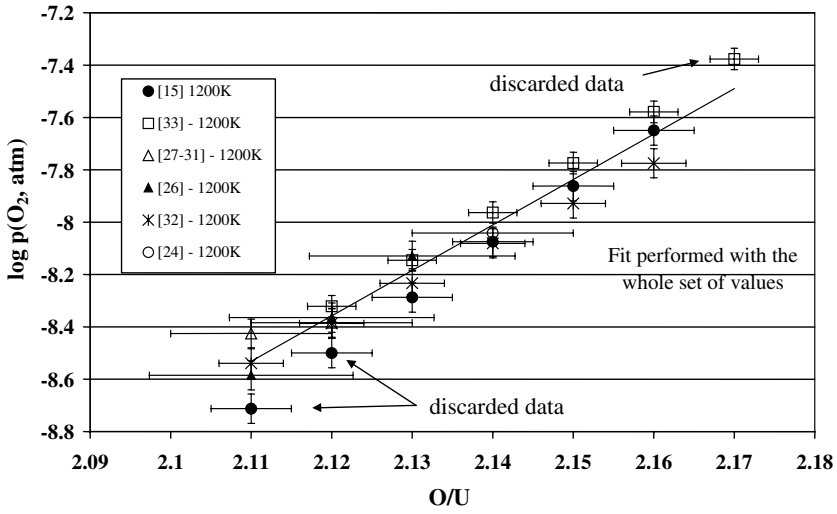

Fig. 7. Comparison of the oxygen pressure decimal logarithms obtained from the chart at 1200 K and for different authors in the 2.11–2.17 O/U range. The uncertainty bars are those estimated in this work for the original measurements.

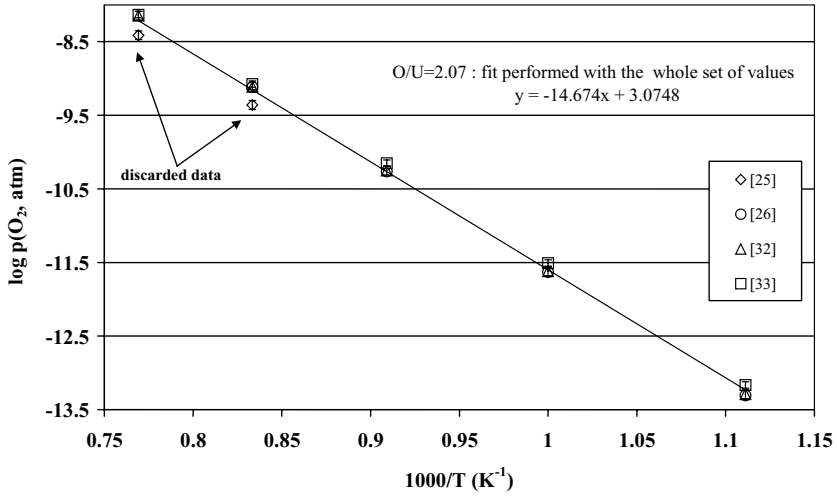

Fig. 8. Oxygen potential decimal logarithm comparison between our chart results obtained from different e.m.f. studies for the $O/U = 2.07$ composition as a function of the inverse of temperature. Uncertainty bars as estimated in this work.

Fig. 7 shows the different chart data (nodes T, x) obtained for one temperature (1200 K), each set of data being quoted with the original estimated uncertainty associated with the set. Discarded chart data are those for which the mean fitted value does not fall within our uncertainty bar. The same analysis is performed as a function of the inverse of temperature as shown in Fig. 8.

As a conclusion, chart data that are retained correspond to a consistent set of e.m.f. experimental data. Those few data that are discarded are neither the whole set of data of an author but are from individual experiments or some of the data, their significant shift from the mean value coming probably from an undetected extraneous reaction or an erratic uncertainty in the determinations of T, x or e.m.f.

4. Heterogeneous equilibria measurements

Two experimental techniques were used:

- The Knudsen effusion method, which is calibrated by continuous measurement of the cell weight (in a

Table 5
Partial pressures of O_2 obtained by heterogeneous equilibria. Techniques, experimental conditions and uncertainties

Authors [Ref.]	Experimental techniques	O/U measurements uncertainty	Temperature range (K)	$\frac{\delta p_{O_2}}{p_{O_2}}$	Comments
Roberts and Walter [37]	• Thermogravimetry • O_2 quantities by increments measured by McLeod gauge	• $2.10 < O/U < 2.3$ • Calcination at 850 °C, air into U_3O_8 • Or CO reduction and CO_2 analysis • $\delta x = \pm 0.002$ (Authors)	1220–1750 Calibrated thermocouple $\delta T \pm 5$ K (our estimate)	• Uncertainty of the authors • $\delta p_{O_2}/p_{O_2} = \pm 5\%$	• UO_2 initially vacuum degased at 1200–1400 °C
Hagemark and Broli [38]	• Thermogravimetry • Controlled p_{O_2}: $Ar + O_2$ for $p_{O_2} > 10^{-3}$ atm or CO/CO_2 mixtures	• $2.0 < O/U < 2.25$ • In situ gravimetry reference UO_2 at 900 °C with 46% CO/CO_2 • $\mathrm{Log}_{10}\ \delta x = 1.24x - 2.948$ (our estimate)	1173–1773 $\delta T = \pm 5$ K (our estimate)	• For $Ar + O_2$: • $\delta p_{O_2}/p_{O_2} = \pm 2.3\%$ • For CO/CO_2: $\frac{\delta p_{O_2}}{p_{O_2}} = \pm 3.6\%$ (our estimate)	• Mullite furnace may modify the steady-state p_{O_2} pressure (see text)
Gerdanian and Dodé [17]	• Thermogravimetry • Controlled p_{O_2} by CO/CO_2 mixtures	• $2.0 < O/U < 2.18$ • Gravimetry by air oxidation at 800 °C in situ $\rightarrow U_3O_8$ • $\delta x = \pm 0.0015$ (Authors estimate)	1176–1373 $\delta T = \pm 5$ K (our estimate)	• $\frac{\delta p_{O_2}}{p_{O_2}} = \pm 2.5\%$ (our estimate)	• For $x \rightarrow 0$, the accuracy is improved
Kotlar et al. [39]	• Thermogravimetry • Controlled O_2 pressure in $N_2 + O_2$ mixtures	• $2.19 < O/U < 2.63$ • Gravimetry by air oxidation at 800 °C in situ $\rightarrow U_3O_8$ • $\delta x = \pm 0.0015$ (authors estimate)	1383–1435 $\delta T = \pm 2$ K (authors estimate)	• $\frac{\delta p_{O_2}}{p_{O_2}} = \pm 5\%$ (our estimate)	• The N_2 gas may create some oxynitride of U
Anthony et al. [40]	• Thermogravimetry • $O_2 + N_2$ mixtures • Quenched at the end for XRD analysis	• $2.18 < O/U < 2.68$ • Gravimetry with $UO_2 + H_2$, 1000 K as a reference • $\delta x = \pm 0.01$ (authors estimate)	1500–2000 $\delta T = \pm 5$ K (our estimate)	• $\frac{\delta p_{O_2}}{p_{O_2}} = \pm 5\%$ • (our estimate)	• The $N_2 + O_2$ mixing method not detailed
Ackermann and Chang [19]	• Thermogravimetry • $Ar + O_2$ mixture or Cu/CuO equilibrium	• $2.61 < O/U < 2.667$ • Gravimetry with reference U_3O_8, stoichiometric, $p_{O_2} = 0.21$ atm, 870 K • $\delta x = \pm 0.002$ (authors estimate)	843–1445 $\delta T = \pm 5$ K (our estimate)	• $\frac{\delta p_{O_2}}{p_{O_2}} = \pm 35\%$ (Our estimate based on the scatter of the two experiments with gas mixtures)	• See text for uncertainty analysis

Matsui et al. [41]	• Thermogravimetry • $Ar+O_2$ mixtures	• $2.63 < O/U < 2.66$ • Gravimetry with reference UO_2 under H_2 at 1273 K • $\delta x = \pm 0.0002$	1000–1300 $\delta T = \pm 5$ K (our estimate)	• $\frac{\delta p_{O_2}}{p_{O_2}} = \pm 2.3\%$ (our estimate)	• Mass flow calibrated by electrical conductivity of a CoO_{1-x} wire
Carneiro and Abriata [42]	• Thermogravimetry • $Ar+O_2$	• $2.60 < O/U < 2.63$ • Gravimetry with reference UO_2 under H_2 at 1173 K • $\delta x = \pm 0.0002$ (authors estimate)	844–1371 $\delta T = \pm 5$ K (our estimate)	• $\frac{\delta p_{O_2}}{p_{O_2}} = \pm 2\%$ (our estimate)	• Observation of hysteresis when cycling • Attributed to slow kinetics of phase transformations
Blackburn [43]	• Knudsen effusion in a thermobalance • Pt cells	• $2.15 < O/U < 2.55$ • In situ gravimetry • 800 °C, 0.21 atm O_2 • Carrier gas unknown • Ackerman correction done • $\delta x = \pm 0.0067$ (Our estimate)	1263–1399 $\delta T = \pm 5$ K (our estimate)	• Correction for an evaporation coefficient by Blackburn (+9.3%) • $\delta p_{O_2}/p_{O_2} = \pm 18\%$ (Our estimate)	• Our estimate of uncertainty is done in order to overlap the scatter of data • The author neglected the UO_3(g) vaporization

thermobalance), gives the vapor pressure and the instantaneous composition from assumptions on the composition of the effused gas.

- The thermogravimetry in which the temperature or the O_2 pressure is maintained constant. Scanning the other variable allows the determination of the steady-state equilibrium of the sample which corresponds to a constant recorded mass. The mass gain or loss from an initial or final known composition gives the concentration at that time.

Publications related to these methods are presented in Table 5 together with our assigned uncertainties, which are discussed hereafter author by author due to large differences in the applied techniques.

4.1. Blackburn data by the effusion method [43]

From the assumption of an O_2(g) molecule largely predominant in the gas phase, the O_2 pressure (p_{O_2}) is determined by the Hertz–Knudsen relation:

$$p_{O_2} = \frac{\Delta m}{tCs}\sqrt{\frac{2\pi RT}{M}}, \tag{10}$$

Δm being the mass loss of the sample or cell during an experiment run at temperature T during time t. M is the molar mass of the effused species O_2, R the gas constant, C and s the Clausing coefficient and the cross-section of the effusion orifice. Consequently,

$$\frac{\delta p}{p} = \sqrt{\left(\frac{\delta \Delta m}{\Delta m}\right)^2 + \left(\frac{\delta s}{s}\right)^2 + \left(\frac{\delta t}{t}\right)^2 + \left(\frac{\delta C}{C}\right)^2}, \tag{11}$$

formula that generates a total uncertainty of $\cong 2.5\%$ for $\delta t/t = \delta \Delta m/\Delta m \cong 1\%$, $\delta C/C \cong 0.1\%$ and $\delta s/s \cong 2\%$. The uncertainty on the Clausing coefficient corresponds to original calculation, which has been further checked [44]. However, the scatter of Blackburn's data is within $\pm 18\%$, a value that includes also the influence of temperature uncertainty on the O_2 pressure. This last cause of uncertainty can be evaluated using the Clausing–Clapeyron law:

$$\frac{\partial \ln p_{O_2}}{\partial\left(\frac{1}{T}\right)} = -\frac{\Delta_{vap}\overline{H}_{O_2}}{R}, \tag{12}$$

relation in which $\Delta_{vap}\overline{H}_{O_2}$ corresponds to the diphasic domain U_3O_8–U_4O_9 in the Blackburn work. Relation (12) becomes at 1000 K,

$$\frac{\delta p}{p} = \pm 17\,096\,\delta T/(1000)^2 \tag{13}$$

and with $\delta T = \pm 2$ K as proposed by Blackburn, we calculate $\delta p/p \cong 3.4\%$. Adding the two uncertainties evaluated by relations (11) and (12), we explain only

±5% of the ±18% observed scatter in the Blackburn data.

The experimental large scatter may have different origins that we tentatively list as follows:

- The interpretation of mass loss via the Hertz–Knudsen equation is not straightforward since there exist a non-negligible residual pressure (O_2 mainly coming from effusion) in the apparatus due to a small vacuum conductance. Blackburn added this measured pressure – probably in a cold part of the apparatus – to the deduced pressure from the Hertz–Knudsen equation. In fact, as we have studied these phenomena in case of oxide vaporization [45], the real and accurate equation becomes,

$$\Delta m = \frac{sC\sqrt{M}}{\sqrt{2\pi R}}\left(\frac{p(\text{effusion})}{\sqrt{T_{\text{eff}}}} - \frac{p(\text{vacuum})}{\sqrt{T_{\text{room}} = 300}}\right)\Delta t \tag{14}$$

  and the correction applied by adding the residual pressure to the measured one (by mass loss) becomes in fact about twice the residual pressure. The above equation represents, in fact, the so-called 'thermomolecular effect' [46]. This correction increases the Blackburn pressures by 3% at 1250 K to 0.8% at 1400 K.
- The genuine effusion phenomenon, as evaluated by the Clausing coefficient and the Hertz–Knudsen relation, may be disturbed by other processes occurring near or at the effusion orifice. Such processes are surface diffusion along the orifice wall [47–49], or bulk diffusion of O through the cell lid or walls [48], since the crucible is not surrounded by a thick envelope as it is in the conventional Knudsen method. These processes may add a supplementary outgoing flow of matter, which is monitored by the balance. The consequence would be to increase the calculated pressure, but not to influence the deduced instantaneous compositions as measured by continuous weight loss.
- The existence of an evaporation coefficient that Blackburn proved when measuring with two different orifice sizes – a larger orifice gives a lower pressure – means that the sample vaporization is 'hindered' by some kinetic phenomenon occurring at the surface of the sample. As the scatter seems larger at low temperature and at the begining of the experiments, the vaporization kinetics may lead to some instable period that depends on the characteristics of the samples – powder, grains, polycrystals ... – or on the history of the samples – sintering or ageing processes – as we have observed directly by mass spectrometry on $Si + SiO_2$ or SiO_2 powders [50].
- The assumption of a gas phase composition largely dominated by O_2(g), has been further contested by Kotlar et al. [36] who attributed some mass loss at high temperature (in thermogravimetry) to the UO_3(g) molecule. In this case, relation (10) becomes,

$$\Delta m(\text{meas}) = \frac{sC}{\sqrt{2\pi RT}}\left[\sqrt{M_{O_2}}p_{O_2} + \sqrt{M_{UO_3}}p_{UO_3}\right]\Delta t. \tag{15}$$

- So, at high temperature any appearance of UO_3 (g) will lead to an overestimate via relation (10) of the oxygen pressure as calculated using the mass loss by Blackburn. Some discrepancies exist for the stability data of the UO_3(g) molecule. In a mass spectrometric PhD study by Younès [51], directed by Pattoret and Nguyen, a careful analysis of fragmentation patterns as well as the determination of ionisation cross-sections ratio $\sigma(UO_3)/\sigma(UO_2) = 3 \pm 0.5$ led to a new and more stable enthalpy of formation value: $\Delta_f H^0(UO_3, g, 298\ K) = -833 \pm 16\ \text{kJ mol}^{-1}$. Using data of Cordfunke and Konings [52] for the U_3O_8(s), U_4O_9(s) and UO_2(s) oxides, the O_2(g) and UO_3(g) partial pressures are calculated for the diphasic U_3O_8(s)–U_4O_9(s) and UO_2(s)–U_4O_9(s) domains (Table 6), as well as the derived quantities:

$$\frac{\text{O mass loss from } O_2}{\text{Total mass loss}} = \frac{p_{O_2}\sqrt{M_{O_2}}}{p_{O_2}\sqrt{M_{O_2}} + p_{UO_3}\sqrt{M_{UO_3}}} \tag{16}$$

  and

$$\frac{\text{O total mass loss}}{\text{Total mass loss}} = \frac{p_{O_2}\sqrt{M_{O_2}} + p_{UO_3}\frac{3M_O}{\sqrt{M_{UO_3}}}}{p_{O_2}\sqrt{M_{O_2}} + p_{UO_3}\sqrt{M_{UO_3}}}. \tag{17}$$

  Relation (16) evaluates the true value of mass loss due to O_2 reported to the total mass loss (in Hertz–Knudsen relation (10)) that is the real p_{O_2} pressure compared to the original p_{O_2} pressure deduced by Blackburn, meanwhile relation (17) evaluates the true relative mass loss of oxygen compared to the total mass loss used in the determination of the O/U composition by Blackburn. The errors δx are calculated for the U_4O_9 composition ($UO_{2.25}$) and δx_1 for the UO_{2+x} phase boundary (Table 6).
  Thus, we can deduce that:

- The O_2(g) pressure at the beginning of the experiment is over-evaluated by 2–4% in the 1239–1399 K temperature range of the experiments, from relation (17).
- The mass loss is in error by 1–3% in the first step of the effusion experiments; the crossing of the diphasic domain leading to a systematic composition shift towards the U rich compositions. For a Blackburn sample of 0.65 g, the systematic error on the mass loss when crossing the diphasic region varies from 0.042 (1%) to 0.0125 (3%). This systematic error will be discussed later in paper II of this series in relation to the limits of the non-stoichiometric domains.

Table 6
Partial pressures of O_2(g) and UO_3(g) calculated for the diphasic U_3O_8–U_4O_9 and UO_2–U_4O_9 domains and the impact on mass loss of O_2 or total oxygen as compared to the total one measured by Blackburn [43]

T (K)	Diphasic U_3O_8–U_4O_9					Diphasic UO_{2+x}–U_4O_9		
	$\mathrm{Log}_{10} p_{O_2}$ (bar)	$\mathrm{Log}_{10}\ p_{UO_3}$ (bar)	$\frac{\Delta_m(O_2)}{\Delta_m(tot)}$ relation (16)	$\frac{\Delta_m(O\,tot)}{\Delta_m(tot)}$ relation (17)	δx at U_4O_9 composition	$\mathrm{Log}_{10} p_{O_2}$ (bar)	$\mathrm{Log}_{10} p_{UO_3}$ (bar)	δx_1 at UO_{2+x} composition
1239	−5.068	−7.324	0.984	0.986	0.006	−7.835	−8.362	0.007
1263	−4.820	−7.014	0.981	0.984	0.007	−7.600	−8.057	0.008
1277	−4.680	−6.839	0.980	0.983	0.007	−7.466	−7.884	0.008
1285	−4.601	−6.741	0.979	0.982	0.007	−7.392	−7.787	0.009
1309	−4.370	−6.454	0.976	0.980	0.008	−7.173	−7.505	0.009
1323	−4.240	−6.291	0.974	0.978	0.009	−7.050	−7.345	0.010
1331	−4.167	−6.200	0.973	0.978	0.009	−6.980	−7.255	0.010
1353	−3.969	−5.955	0.970	0.975	0.010	−6.794	−7.014	0.011
1373	−3.796	−5.739	0.967	0.975	0.011	−6.630	−6.802	0.012
1376	−3.770	−5.708	0.967	0.972	0.012	−6.606	−6.771	0.012
1399	−3.578	−5.469	0.963	0.969	0.013	−6.424	−6.536	0.013

The impact δx on the $(2+x)$ composition corresponding to the U_4O_9 compound is calculated as well as at the UO_{2+x} phase boundary. (Blackburn compositions: $(2+x)$ becomes after correction $(2+x+\delta x$ or $2+x+\delta x_1))$.

However, as we shall see further, even if the Blackburn O_2 pressure data seem too high by a few percentage, the 18% scatter (adopted by us as the uncertainty in this work) favours overlaping with other data. In addition, the impact of any matter loss by UO_3(g) on the composition may be important and the shift of compositions towards U appears greater than the uncertainty quoted by the author for the composition: 0.25%, that is $\delta x = 0.0067$. Moreover we observe that Blackburn data when oxidizing UO_2 into U_3O_8 were within this 0.25% although at this temperature (1073 K) the stoichiometric composition could not be reached according to Ackerman and Chang [19]. As the corrected formula for U_3O_{8-z} gives the same 0.25%, the final uncertainty adopted here is twice, $\delta x = \pm 0.0067$, independently of the above systematic calculated error.

4.2. Roberts and Walter [37]

The pressure of O_2 is determined with a McLeod gauge. The uncertainty may come from the reading of the height of a mercury column, and the determination of the exact volume of the reactor and manometer tube. We estimate this uncertainty at about ±5%, a value, which matches the scatter of the data. We quote that the authors have made corrections for the isopiestic equilibrium (thermomolecular effect) of the O_2 gas between the hot and cold parts of the vessel: these corrections effectively draw the original raw data towards a more meaningful thermodynamic evolution of the O_2 pressure for a monophasic domain as a function of temperature.

4.3. Hagemark and Broli [38]

The U–O system was studied by thermogravimetry with controlled oxygen potential: $Ar + O_2$ mixtures for $p_{O_2} > 10^{-3}$ bar, and CO/CO_2 equilibrium for lower oxygen potentials. The composition uncertainty during the measurements is evaluated as follows:

- For $O/U = 2.05$, the uncertainty corresponds to the reproducibility, $\delta x = \pm 7 \times 10^{-4}$.
- For $O/U = 2.25$, the UO_3(g) vaporization as quoted by the authors, leads to $\delta x = \pm 10^{-3}$.
- An uncertainty for reading the graphs is added: $\delta x = \pm 5 \times 10^{-4}$.
- The uncertainty on the gravimetric reference. There are two references: (i) oxidation in situ into U_3O_8, (ii) volumetric analysis of CO_2 issued from the UO_2 reduction under CO pressure. The agreement between these two methods is ±0.002, which is considered as the uncertainty derived from the references.

On the basis of the total uncertainty calculated according to the law of propagation of errors for $x = 0.05$ $(\delta x = 2.17 \times 10^{-5})$ and $x = 0.25$ $(\delta x = 24 \times 10^{-4})$, we obtain for the composition uncertainty the relation:

$$\log_{10} \delta x = 0.2188x - 2.6745. \quad (18)$$

The total uncertainty on the p_{O_2} determination depends on the gaseous mixture that is used. For the $Ar + O_2$ mixture, the reading uncertainty is ±2.3%, and the one for the mass flow is ±0.4%. Thus, $\delta p_{O_2} = \pm 2.33\%$. For the CO/CO_2 mixture, the reading accuracy on the graph

is the same, ±2.3%, for the mass flow ±1% because two gases are monitored, and finally we must add the uncertainty issued from the equilibrium constant K_p for the reaction,

$$CO_2 = CO + (1/2)O_2. \tag{19}$$

Hagemark and Broli used $\log_{10} K_p = -14757/T + 4.528$ in the 1100–1800 K range, relation different from the one issued from JANAF tables [53], $\log_{10} K_p = -14675/T + 4.4862$. Consequently, and to obtain a consistent set of data, we corrected their original results using the JANAF equilibrium constant. Then, the uncertainty for equilibrium (19) is calculated from the relation,

$$\Delta_r G(CO/CO_2) = -2.303RT\log K_p = \Delta_r H - T\Delta_r S, \tag{20}$$

that gives, applying the law of propagation of errors,

$$\frac{\delta K_p}{K_p} = \sqrt{\frac{(\delta\Delta_f H_{CO})^2 + (T\delta\Delta_f S_{CO})^2 + (\delta\Delta_f H_{CO_2})^2 + (T\delta\Delta_f S_{CO_2})^2}{(2.303RT)^2}}, \tag{21}$$

the uncertainties associated with $\Delta_f H^0$ and $\Delta_f S^0$ of formation of CO and CO_2 being taken from JANAF tables. By this approach, we admit that there are no uncertainties considered associated with C_p^0 of these gases, the uncertainties being totally reported on enthalpies and entropies at 298 K. The calculated uncertainty $\delta K_p/K_p$ varies from 1.1% at 1100 K to 0.9% at 1800 K. We chose $\delta K_p/K_p = \pm 1.1\%$, and the total uncertainty associated to the determination of oxygen pressure by the CO/CO_2 equilibrium in the Hagemark and Broli work becomes,

$$\delta \log p_{O_2} = \sqrt{(2\delta K_p/K_p)^2 + 2(\delta(CO/CO_2)/(CO/CO_2))^2 + \delta(\text{readings})^2} = \pm 3.6\%.$$

One more problem remains in the Hagemark and Broli work: the use of an oxide (Mullite) as a laboratory tubing, in a wide range of temperature and oxygen potential. As the mass of this material is more important than the one of the sample and also than the local instantaneous gas density, one can question about the final steady-state of not only the sample, but of the whole system gas + sample + furnace tubing [54]. In order to evaluate a possible impact of the furnace tubing material on the gaseous equilibria, we calculated the congruent vaporization of Mullite and compared with the operating oxygen pressures. The congruent vaporization of Mullite corresponds in fact to the main gaseous species SiO(g), O(g) and O_2(g), in such a composition that the gas phase can move with non-stoichiometric oxygen composition evolution of the condensed phase: the mass loss of the Mullite enhances a composition evolution along the pseudo-binary line SiO_2–Al_2O_3, towards Al_2O_3 which is the less volatile compound. Mechanism of such pseudo-congruent vaporization has been already explain for other similar systems [45]. After a while and due to SiO_2 mass loss, Mullite produces Al_2O_3 and the congruent vaporization conditions are those of the diphasic Mullite–Alumina for which calculated oxygen partial pressures according to JANAF [53] correspond to the equation:

$$\log_{10} p_{O_2}/\text{bar}(\text{mullite, congruent}) = -27\,352.3/T + 7.6457. \tag{22}$$

This oxygen congruent (or pseudo-azeotropic) pressure must be compared to imposed conditions by the gas flow in the furnace tubing as illustrated in Fig. 9. For gas flow the oxygen pressure of which is higher than the congruent one, in the initial stage of the experiment, the Mullite tubing will adsorb the oxygen and the Mullite composition moves towards oxygen rich side in its non-stoichiometric domain. As this domain in this compositional direction is very small, this evolution must be quite rapid. The last step of this evolution may be slowed by a diffusion process of oxygen through the tubing walls from the outside atmosphere. When the imposed oxygen pressure increases, this diffusion flow decreases due to the smaller gradient of oxygen potential through the wall of the furnace tubing.

Conversely, when imposing lower oxygen pressures than the congruent one, Mullite tends to vaporize congruently and consequently to enrich the gas with oxygen (as well as SiO(g)) in a first step. As these sorts of experiments are generally performed during a long time in order to obtain equilibrium conditions, finally the oxygen sink in quasi-stoichiometric Mullite will become insufficient and Mullite or its surface layer should be reduced. The diffusion of oxygen from outside is at that time favored by a larger chemical potential gradient. Consequently it is in these ranges that some trends may appear, the attended oxygen potential corresponding to the input gas flow could not be attained, and the UO_{2+x} composition – as measured independently – would correspond to truly higher O_2 pressures. In order to detect some impact of these phenomena, we compare in Fig. 10 the Hagemark and Broli data at 1373 K with those of Gerdanian and Dodé [17]. In this case, for higher pressures than the congruent one, the systematic composition shift of Hagemark and Broli could allow us to suppose that Mullite allows oxygen diffusion through the furnace walls (the oxygen composition appears higher for the same imposed oxygen potential). Although this systematic difference is observed between these two sets of data,

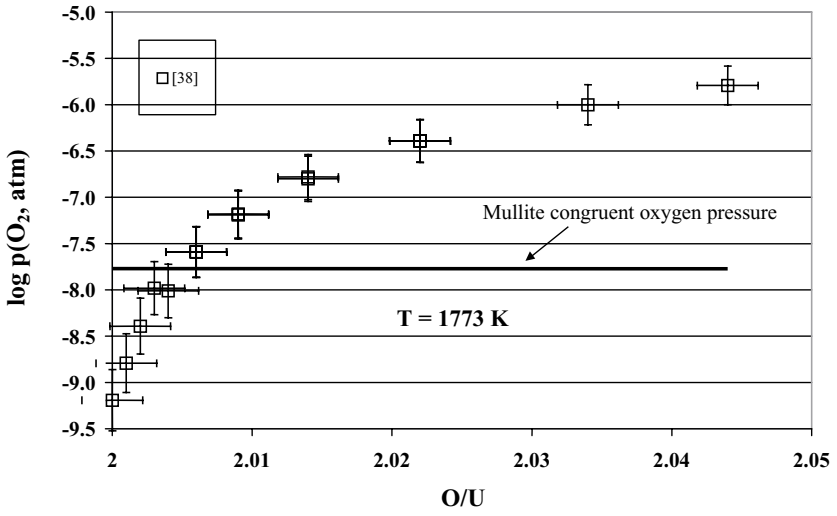

Fig. 9. Comparison of the oxygen pressure of the congruent vaporizing Mullite with the oxygen pressures measured by Hagemark and Broli [38].

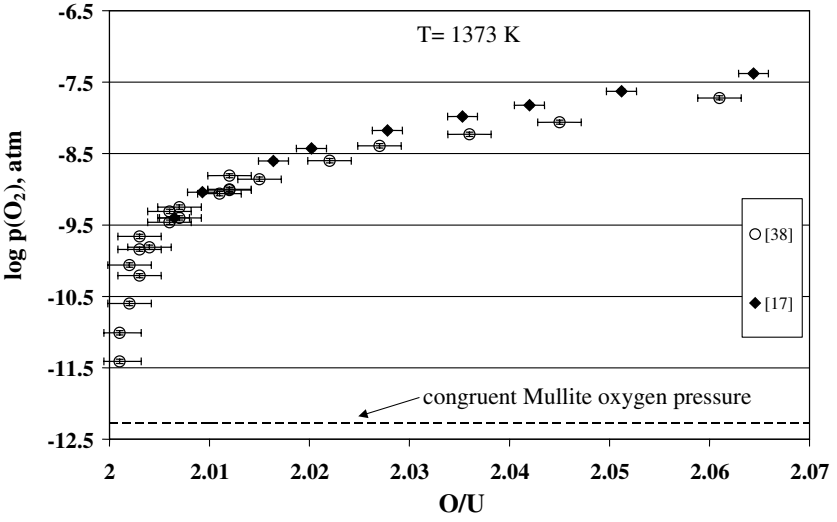

Fig. 10. Comparison of Hagemark and Broli [38] and Gerdanian and Dodé [17] results obtained at 1300 K. The values of these two authors are considered to agree within their uncertainty limits although we observe a systematic shift between the data of these authors.

this difference cannot serve as selection criteria since the uncertainty ranges always overlap.

4.4. Gerdanian and Dodé [17]: thermogravimetry

The oxygen potential is controlled with CO/CO_2 mixtures. The as printed values have been recalculated using the JANAF tables [53] for consistency. The uncertainty analysis is the same as for the preceding authors:

- Uncertainty for the mixing of gases: ±0.4% (authors).
- Uncertainty due to the gas purity: ±1%.
- Uncertainty in the equilibrium constant: ±1.1%.

As the law of propagation of errors leads to a very small and unrealistic uncertainty (±1.5%), we simply summed these uncertainty values:

$$\delta \log p_{O_2} = \frac{\delta p_{O_2}}{p_{O_2}} = \pm 2.5\%. \quad (23)$$

This last choice is further confirmed by the difficulties encountered later by Kotlar et al. [39].

4.5. Kotlar et al. [39]: thermogravimetry

The O_2 pressure is controlled by $N_2 + O_2$ mixtures in the same apparatus as in part 4.4. The reproducibility is ±0.4%, but the determination of the pressures for the diphasic regions – U_3O_8–U_4O_9 and UO_{2+x}–U_4O_9 – are bracketed within an uncertainty range of ±5%. Although the appearance of a second phase can necessitate an activation energy and consequently an excess or deficit of oxygen – depending on the way of running the experiment – which are included in the ±5%, we reasonably prefer to keep this uncertainty range for all the data of Kotlar et al. Indeed, some 'negative bracketed' values show that the uncertainty of measurements is clearly as large as the excess (or deficit) pressure for activation.

The uncertainty on the composition is due to the thermobalance reproducibility, $\pm 5 \times 10^{-4}$, added with the experimental reproducibility, $\pm 10^{-3}$: total $\delta x = \pm 1.5 \times 10^{-3}$.

4.6. Anthony et al. [40]: thermogravimetry

Same technique than Kotlar et al. with $N_2 + O_2$ mixtures and due to the absence of details, we chose $\delta p_{O_2}/p_{O_2} = \pm 5\%$ by analogy. We adopt their uncertainty on composition: $\delta x = \pm 0.01$.

4.7. Ackermann and Chang [19]: thermogravimetry

Depending on the working O_2 potentials, the authors used:

- $Ar + O_2$ mixtures (for $p_{O_2} = 10^{-3}$–1 atm), without any published accuracy. We arbitrarily chose $\delta p_{O_2}/p_{O_2} = \pm 1\%$.
- CuO/Cu_2O equilibrium ($p_{O_2} < 10^{-3}$ atm). The oxygen potential uncertainty is estimated as for the CuO/Cu_2O equilibrium, and according to JANAF values [53]. The original Ackermann and Chang data are first corrected according to JANAF tables. Finally, $(\delta K_p/K_p)(CuO/Cu_2O) = \pm 19\%$ at 800 K and ±10% at 1500 K
  and

$$\frac{\delta p_{O_2}}{p_{O_2}} = \left[\left(2\frac{\delta K_p}{K_p}\right)^2\right]^{0.5} = \pm 20\text{–}38\%.$$

The data are scattered within ±13%–±35%, and no trend due to temperature seems to occur. Moreover, the authors performed their measurements by increasing or decreasing values without any significant differences. For these reasons we retain ±35% as an upper limit for uncertainties, a limit which agrees with the one attributed to the CuO/Cu_2O equilibrium uncertainty.

5. Comparison of data sets of different techniques

As the different sets of raw data are not conveniently overlapping – even when their temperature and composition ranges overlap – we use a chart, as already explained, for e.m.f. data interpretation. This analysis must be performed only for solution phases and the first step is the analysis of phase limits.

5.1. Biphasic domains UO_{2+x}/U_4O_9 or U_3O_8

Fig. 11 shows the chemical potentials as a function of the inverse of T, and a very good agreement between all sets of data – including those from e.m.f. measurements – for the UO_{2+x} phase limit, upper oxygen phase boundary. At higher temperature, as shown in Fig. 12, the least-square fit of phase-boundaries compositions – corresponding to different diphasic domains – gives a decomposition temperature $T = 1393$ K for U_4O_9 into UO_{2+x} and U_3O_8. This result agrees with 1390 ± 8 K as proposed in paper II. These fits will not be used further since the optimization procedure needs each set of raw data. The Kotlar et al. data [39] show p_{O_2} apparently too large after evaluation, and we no longer retain these data.

5.2. Monophasic UO_{2+x} domain

When building a chart of these data and comparing with e.m.f. data, firstly we can conclude the following:

- Figs. 13 and 14 show that oxygen potentials values of Gerdanian and Dodé [17] are slightly higher than for other authors. We believe that N_2(g) may react with UO_2. The opposite situation applies for Aronson and Belle [25]. In case of disagreement – the criteria being the present estimate of the uncertainty – these data are discarded. We have to state that we have discarded only series of data, and that we have never completely discarded the data of any authors.
- Agreement between other authors of heterogeneous equilibria measurements is always observed (the preceding heterogeneous equilibria selection being completed) as well as with e.m.f. data in the low temperature range.
- In some ranges – particularly at high temperature – the comparison is not possible due to the small number of data and their large uncertainty as shown in Fig. 15. We have to quote that Anthony et al. data [40] were not entered in the chart, due to too large uncertainties, but these data will be still stored as raw data for the optimization procedure. In addition, some discrepancies occurred between Hagemark and

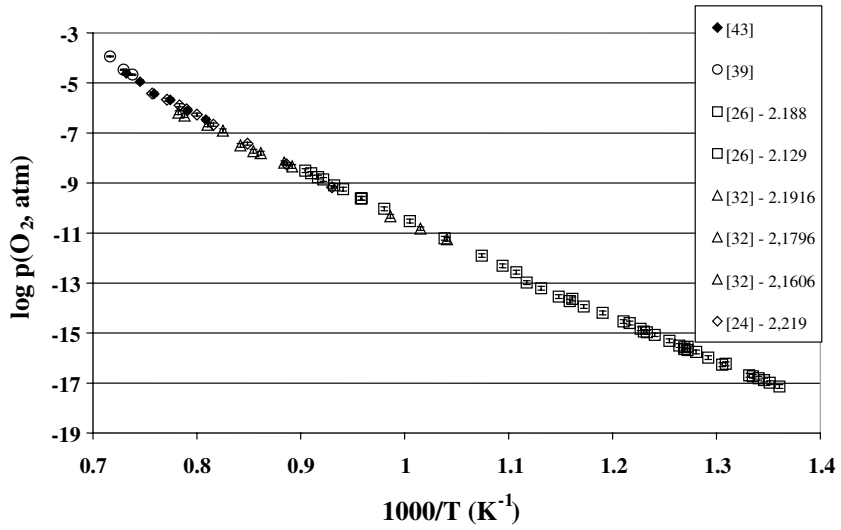

Fig. 11. Experimental decimal logarithm of oxygen potentials measured at the UO_{2+x}–U_4O_{9-y} phase boundary.

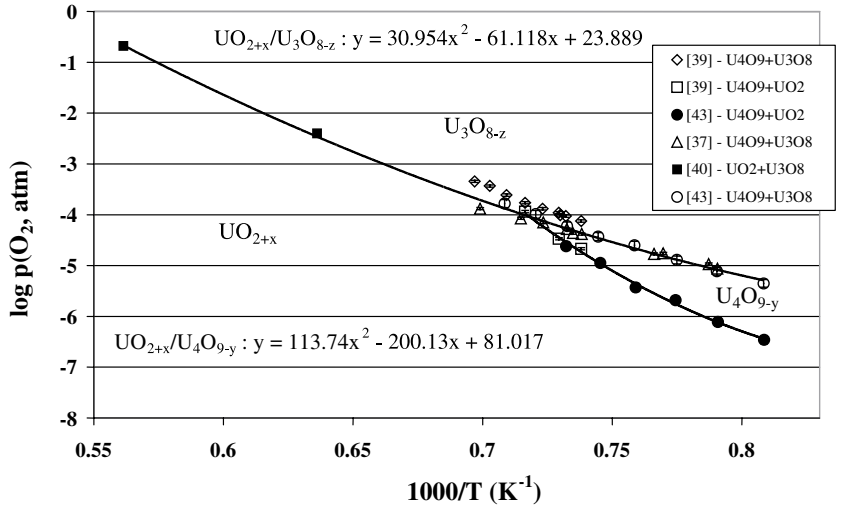

Fig. 12. Least square fit of the phase boundary compositions at high temperatures and decomposition temperature of U_4O_9 into $UO_{2+x} + U_3O_8$.

Broli [38] at high temperature and Roberts and Walter [37]. We believe that the vaporization of UO_3(g) was not realistically calculated for its true value in the correction term, since the $\Delta_f H^0(UO_3,g)$ varies from −799.4 kJ mol^{-1} [52] down to −833 kJ mol^{-1} as redetermined and compiled [51].

5.3. Monophasic U_3O_{8-z} domain

Data for this domain are scarce mainly because e.m.f. measurements are not feasible, and moreover all data sets disagree as shown in Figs. 16 and 17. These features do not allow a direct selection of a minimum set of data.

During isothermal cycling between two imposed O_2 pressures, Caneiro [55] observed some hysteresis phenomenon that he attributed to the formation of new or metastable phases. We believe that this is more probably related to retarded kinetics, which we observe to be greater in Caneiro's work [42] when vaporizing than when condensing and which decreases with temperature increase in his experiments (the usual evolution of activated phenomena). The pressure gap is 10^4 at 844 K, 10^2 at 998 K and finally 0 at 1371 K; values calculated from the Caneiro's graphs. These pressure increments or decrements can be related to the observation of an evaporation coefficient for O_2(g) by Blackburn [43].

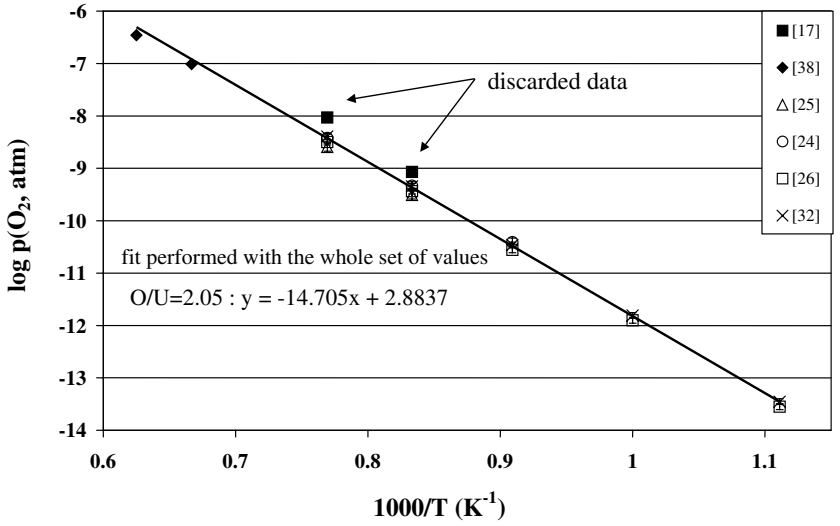

Fig. 13. Evolution of the decimal logarithm of the oxygen pressure according to our chart versus the inverse of temperature for the $O/U = 2.05$ composition, as used for comparison of experimental results.

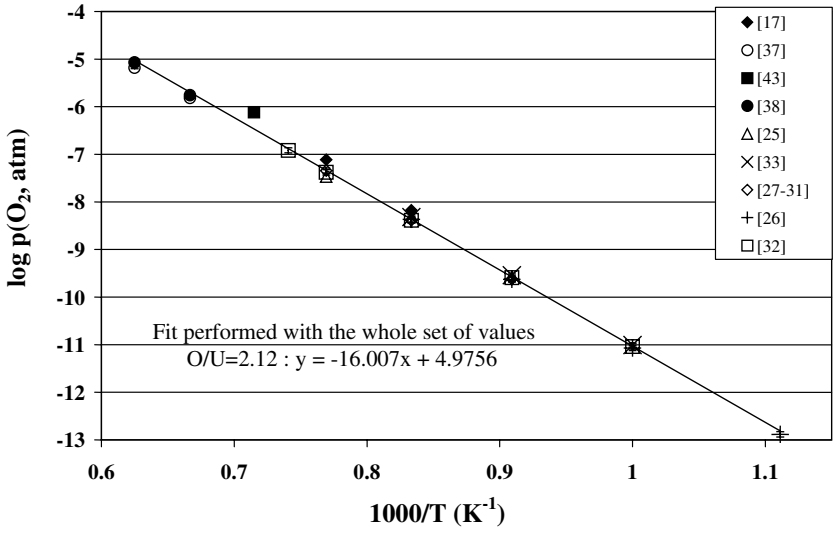

Fig. 14. Evolution of the decimal logarithm of the oxygen pressure according to our chart versus the inverse of temperature for the $O/U = 2.12$ composition, as used for comparison of experimental results.

Indeed, the fact that $O_2(g)$ vaporizes according to a hindered vaporization implies that any steady state of measurement in a thermobalance will be flow dependent. This dependence may be different for oxidation and reduction steps if some condensation coefficient exists with a value different from the one for the evaporation step as already discussed by Rocabois and coworkers [56] in effusion studies. As Caneiro found that the steady-state oxygen potentials for oxidation were systematically higher than those for reduction, this feature means that these two coefficients are different, leading to hysteresis behavior. Ackermann and Chang [19] observed also such a behavior but only at $T > 1196$ K, attributed to probable structural changes, and Matsui et al. [41] observed also numerous slope changes in this range. All these different behaviors may be related to flow conditions in the different apparatus.

The existence postulated by Blackburn [43] of an evaporation coefficient lower than unity (unity at equilibrium), leads us to propose two rules for data selection:

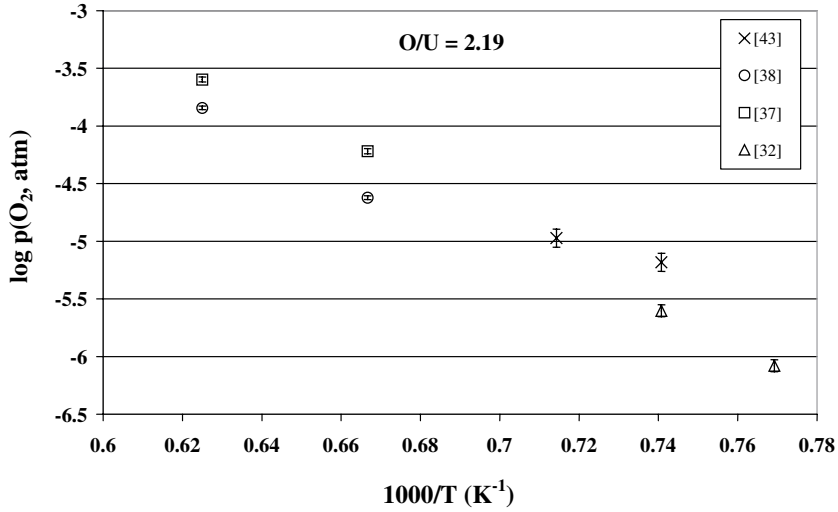

Fig. 15. Evolution of the decimal logarithm of the oxygen pressure according to our chart versus the inverse of temperature for the $O/U = 2.19$ composition, as used for comparison of experimental results.

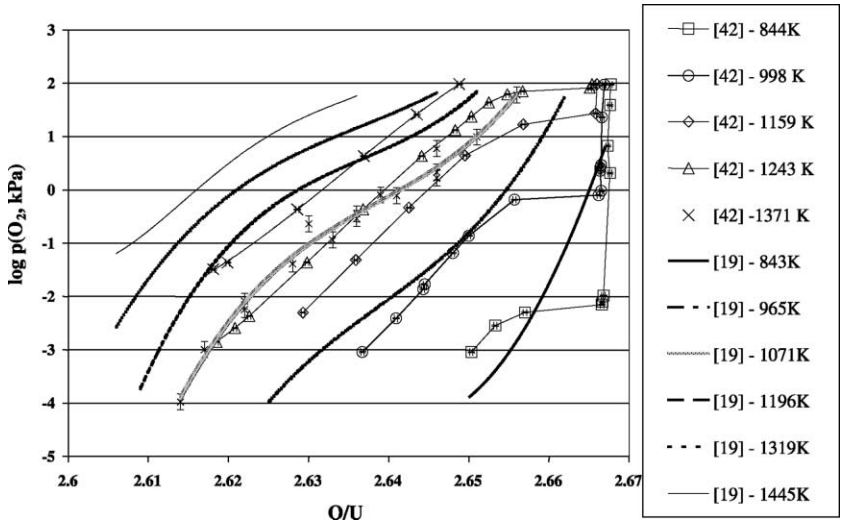

Fig. 16. Decimal logarithm of the oxygen pressure comparison between the Ackermann and Chang [19] and Caneiro and Abriata [42] studies. The oxygen potentials from these two studies are in kPa.

- The retained oxygen equilibrium pressure will be the higher measured one for a given temperature (apparent evaporation coefficient $\rightarrow 1$), or the equivalent rule, the lower the temperature for an imposed oxygen potential in the experiments.
- The retained values in the U_3O_{8-z} monophasic region at its low oxygen phase boundary must be consistent with those retained in the diphasic domain U_4O_9–U_3O_8 for which, the measured oxygen potentials agree whoever the authors.

According to these two criteria, the lone set that we retain is that of Ackermann and Chang. Moreover, their data, obtained by oxidation and reduction, imply the determination of true equilibrium conditions. Indeed, their data show an appropriate merger with those in the diphasic region (Fig. 18). Finally these oxygen potentials are the highest measured ones for a fixed temperature, and all other authors disagree always in the same direction in agreement with the existence of kinetic barriers for vaporization and condensation of $O_2(g)$.

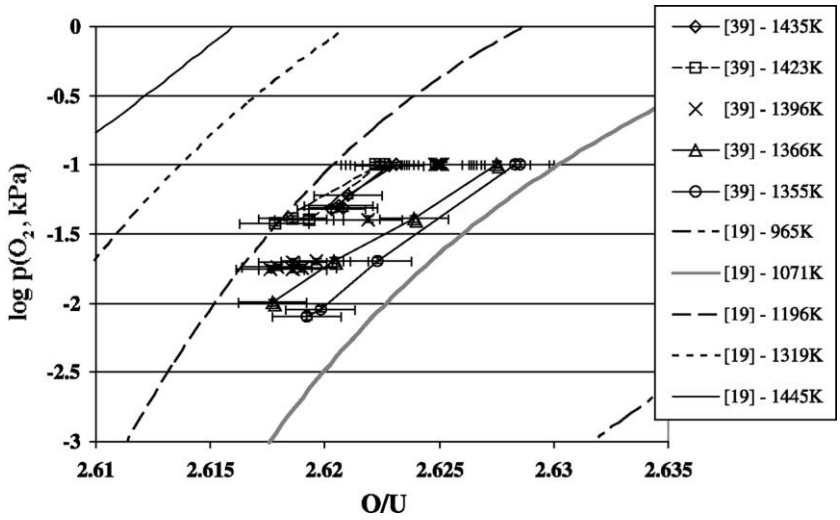

Fig. 17. Decimal logarithm of the oxygen pressure comparison between Ackerman and Chang [19] and Kotlar et al. [39] works. The oxygen potentials from these two studies are in kPa.

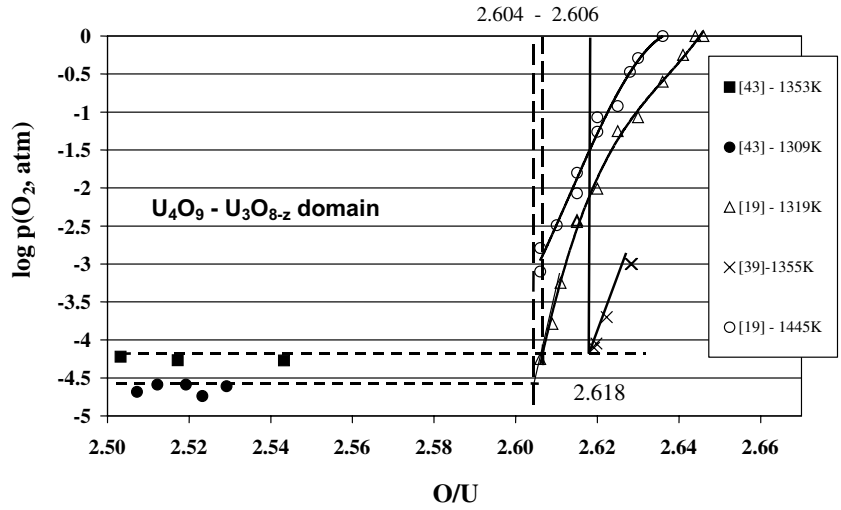

Fig. 18. Analysis of Ackerman and Chang [19] and Kotlar et al. [39] lower oxygen boundary limit for U_3O_{8-z} domain, in relation with the oxygen pressures of the $U_4O_{9-y} + U_3O_{8-z}$ diphasic region.

One important consequence of this choice is the final lower oxygen boundary for the U_3O_{8-z} which appears shifted towards the oxygen rich compositions as shown in Fig. 18 when comparing Kotlar et al. value (discarded) with the value of Ackermann and Chang at 1319 K (retained).

6. Discussion on the analysis of oxygen potentials

The large domain of temperature analyzed for UO_{2+x}, as well as the number of original data required a method for comparing data obtained from three different techniques as well as for a comparison of results from the same technique. Beyond this primary aim, the number of original data needed to be decreased in order to introduce a significant set in the optimization procedure.

For UO_{2+x}, different least square fits were used in order to reduce any data set to the lone nodes of a (T, x) chart. At this stage, the comparison of data allows us to discard some of these data – never the full set of an author for UO_{2+x} domain – on the basis of the total uncertainty analysis performed for the data of each author.

The resulting set of nodes of the chart is presented in Fig. 19 and Table 7 as fits. The phase limit of the diphasic UO_{2+x}–U_4O_9 is consistent with this set as well as the U_4O_9 peritectic decomposition temperature. The agreement between different authors is very good, except for the U_3O_8 compound phase limits and oxygen potentials.

The number of reduced data is presented in Table 8, according to the technique and for the different

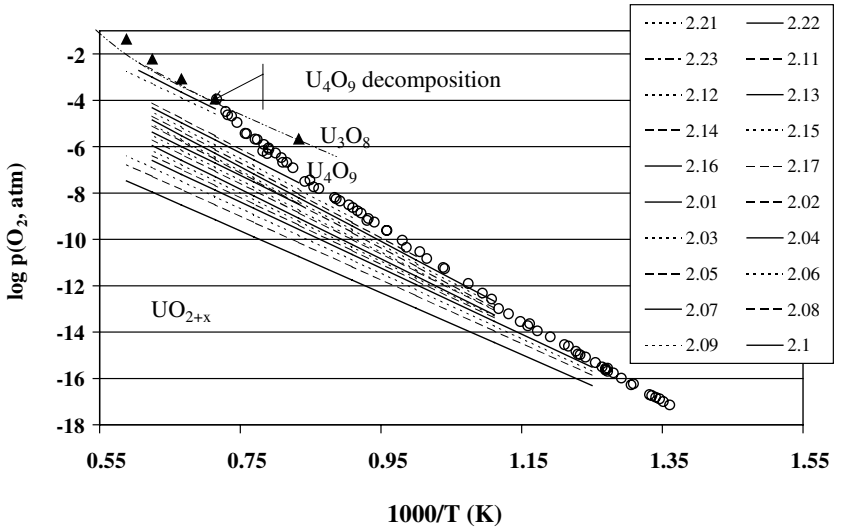

Fig. 19. Representation of the resulting set of nodes of our experimental chart reduced by least square fits.

Table 7
Evolution of the decimal logarithm of O_2 partial pressures (units: atm) as a function of the inverse of temperature ($\log_{10} p_{O_2} = A/T\ (K) + B$) in the UO_{2+x} monophasic domain for different compositions ($2 + x$) according to our treatment of experimental data with constant intervals of a (T, x) chart

UO_{2+x} composition: $2 + x$	A	B	Temperature range (K)
2.01	−13 353.5195	0.3850	800–1700
2.02	−13 733.2788	1.3081	800–1700
2.03	−14 041.6748	1.8735	800–1700
2.04	−14 265.7449	2.3179	800–1600
2.05	−14 407.3480	2.6220	900–1600
2.06	−14 678.5033	3.0126	900–1600
2.07	−15 012.2542	3.4231	900–1600
2.08	−15 143.2628	3.7686	900–1600
2.09	−15 507.5349	4.1864	900–1600
2.10	−14 882.6849	3.9223	900–1600
2.11	−16 171.6625	5.0042	900–1600
2.12	−15 990.8477	4.9583	900–1600
2.13	−16 073.8928	5.1887	900–1600
2.14	−16 157.7242	5.4179	1000–1600
2.15	−16 074.9488	5.5488	1100–1600
2.16	−15 499.6902	5.3590	1200–1600
2.17	−15 915.4307	5.8314	1300–1600
2.18	Not enough data	–	–
2.19	Not enough data	–	–
2.20	Not enough data	–	–
2.21	−14 585.7129	5.8346	1400–1700
2.22	−15 236.4769	6.5092	1400–1650
2.23	−16 127.2861	7.4054	1400–1650

For some composition a fit is not proposed because we do not have enough data. For UO_{2+x}–U_4O_9 and U_4O_9–U_3O_8 diphasic domains, it is not possible to propose a such kind of equation. For a short temperature range, these fits are proposed in Fig. 12.

Table 8
Comparison between the original data number and the final retained chart data number for optimization with Thermocalc–Parrot optimizer

Techniques	Domain of composition	Number of original data	Number of retained data
E.m.f.	UO_{2+x}	670	199
Thermogravimetry and effusion		347	114
E.m.f.	Diphasic UO_{2+x}–U_4O_9	100	64
Thermogravimetry and effusion		27	9
E.m.f.	Diphasic U_4O_9–U_3O_8	0	0
Thermogravimetry and effusion		27	20
E.m.f.	U_3O_8	0	0
Thermogravimetry and effusion		246	53

composition domains. This final selected number of data is quite homogeneous and each data will be weighted by its own original estimated uncertainty because we do not wish to introduce a primary statistical treatment that would interfere with the one included in the optimization procedure. Original data are available either in the form of tables [57] or on electronic diskettes [58] for further optimization procedures.

At the end of this work it is possible to compare our chart results with preceding works of Lindemer and Besmann [2] and Kim [3]. Examples of calculations given in Table 9 show some strong disagreement with our chart. For the monophasic UO_{2+x} domain, our data agree with those of Lindermer and Besmann: this is quite normal because they used the same methodology and build a chart based on all the available data. Small differences are derived from the more rigorous selection that we have performed in this paper in relation with analysis of uncertainties.

The recent work of Kim [3] proposes a new T–C–P (temperature–composition–pressure) chart for the U–O system between UO_2 and U_3O_8. The selection of the phase diagram is based on a restricted selection of few experimental studies. Kim compares the fits based on these experimental results and selects some equations in agreement with an enthalpy constraint and the continuity of the oxygen potential, fitted by a modified form of the Sievert's law at the phase boundaries. This treatment can lead to larger errors as it is illustrated in Table 9 in the case of the monophasic U_3O_{8-z} domain. Moreover, sometimes Kim has not enough data and makes some extrapolations which may be lead to errors: the oxygen potential in the monophasic U_4O_9 domain is obtained by linear interpolation of the data picked at the adjacent phase boundaries. However, as Kim noted, this interpolation does not correspond with the variation law of experimental data. The same kind of treatment has been carried out for U_3O_{8-z}: Kim selected Hagemark and Broli data but in our analysis we have shown this choice is questionable since with the existence of an evaporation coefficient we can ascertain that Hagemark and Broli did not measure the equilibrium pressures. Finally, a great part of the Kim analysis is based on the enthalpy constraint. Applying this, Kim needs to know

Table 9
Comparison between our chart (this study) and the T–C–P relationships determined by Lindemer and Besmann [2] and Kim [3]

Temperature–O/U	Lindemer and Besmann [2]	Kim [3]	This work
Monophasic UO_{2+x} domain			
1200 K–2.01	$p_{O_2} = 6.33 \times 10^{-12}$ atm	$p_{O_2} = 7.39 \times 10^{-13}$ atm	$p_{O_2} = 1.81 \times 10^{-11}$ atm
1200 K–2.05	$p_{O_2} = 4.28 \times 10^{-10}$ atm	$p_{O_2} = 5.83 \times 10^{-11}$ atm	$p_{O_2} = 4.13 \times 10^{-10}$ atm
1200 K–2.15	$p_{O_2} = 1.92 \times 10^{-8}$ atm	$p_{O_2} = 9.46 \times 10^{-9}$ atm	$p_{O_2} = 1.42 \times 10^{-8}$ atm
Diphasic UO_{2+x}–U_4O_9 domain			
800 K	$p_{O_2} = 2.43 \times 10^{-16}$ atm	$p_{O_2} = 2.43 \times 10^{-16}$ atm	$p_{O_2} = 5.09 \times 10^{-16}$ atm
1000 K	$p_{O_2} = 3.09 \times 10^{-11}$ atm	$p_{O_2} = 3.09 \times 10^{-11}$ atm	$p_{O_2} = 3.22 \times 10^{-11}$ atm
1200 K	$p_{O_2} = 7.80 \times 10^{-8}$ atm	$p_{O_2} = 7.80 \times 10^{-8}$ atm	$p_{O_2} = 7.60 \times 10^{-8}$ atm
Monophasic U_3O_8 domain			
843 K–2.65	–	$p_{O_2} = 7.11 \times 10^{-10}$ atm	$p_{O_2} = 1.28 \times 10^{-6}$ atm
965 K–2.651	–	$p_{O_2} = 2.98 \times 10^{-7}$ atm	$p_{O_2} = 3.20 \times 10^{-3}$ atm
1445 K[a]–2.615	–	$p_{O_2} = 2.26 \times 10^{-3}$ atm	$p_{O_2} = 8.80 \times 10^{-3}$ atm

[a] In the temperature range studied by Hagemark and Broli [38].

the phase boundary of each domain to determine the sign of the evolution of the boundaries composition versus the inverse of the temperature: he *never analyses the lower and the upper limits of each domain*, and prefer to choose a rather old version of the phase diagram. For all these reasons, the interesting work of Kim is not really complete since the real shape of the phase diagram have not been analyzed. Facing the complexity of this system, we believe that no short cuts can be taken and the study of this system requires the examination of all the available data with an optimization process, which we have endeavored to present in this paper.

Addenda

During submission of this work, two other works were published [59,60] dealing with thermodynamics of the UO_{2+x} hyperstoichiometric composition range. Kurepin [59] uses one e.m.f. data set (Ref. [32] in this work) and solution thermodynamic modelling to describe the chemical potential of the UO_2 and U_4O_9 species. Conversely, Chevalier et al. [60] selected primary data in order to optimize thermodynamic and phase diagram data for the binary U–O system. Their study is similar to our general aim, the main difference coming from the way of data selection. Our analysis is a sound attempt to operate a more rigorous selection of data before starting any optimization process in order to avoid any trial and error process in the course of optimization. Nevertheless, their set of references indicated some omissions in our work, and we check here after the impact of these omissions in our selection, particularly when comparing with our chart, and only for real primary data.

Thermogravimetric analysis (TGA) of Chapman and Meadows [61] for UO_{2+x} volatility study was interpreted in terms of UO_4(g) preferential vaporization, discarding UO_3(g). This assumption is in complete contradiction with earlier and further mass spectrometric experiments which are the lone to be real analytic measurements. We believe that the assumption of UO_4(g) is working in relation with kinetic limitations as we have postulated

Table 10
Compilations and original studies on the Gibbs energy of the $2Fe(s) + O_2(g) \leftrightarrow 2FeO(s)$ equilibrium

Authors [Ref.]	Nature of the sample	Experimental technique	Chemical reference	ΔG^0_T (J mol^{-1}) and comments
Richardson and Jeffes [65]	Compilation	Heterogeneous equilibria e.m.f. Thermal data		$\Delta G^0 = -519\,234.4 + 125.1T$ 298 K $< T <$ 1642 K
Pankratz [66]	Compilation			$\Delta G^0_T = A + BT$ $\Delta G^0 = 500 < T <$ 1800 K
Kinkkola and Wagner [67]	Fe/FeO	Heterogeneous equilibrium CO/CO_2	CO/CO_2 Coughlin [68]	$\Delta G^0 = -544\,790 + 144.43T$ $1073 < T <$ 1373 K
Kinkkola [69]		Recalculation of the previous work [67]		$\Delta G^0 = -530\,090 + 131.5T$ $1073 < T <$ 1373 K
Takayama and Kimizuka [70]	Starting from Fe_2O_3	TGA for O/Fe determination	p_{O_2} by e.m.f.	$\Delta G^0 = f(x(O))$ for iron oxides
		Heterogeneous equilibria H_2/CO_2		$1173 < T <$ 1573 K
		Control of O_2 potential by e.m.f. cell		
Sjoden et al. [71]	Sintered Fe/Fe_2O_3 into $FeO_{0.95}$	E.m.f. Fe, FeO/ZrO_2 0.18CaO/Ni, NiO	Reference Ni/NiO $\Delta G^0 = -233\,651 + 84.893T$	Discontinuity at 1184 K but small effect on the slope difference
	(Fe/$FeO_{0.95}$) NiO treated in Ar at 1273 K, 12 h (Ni/NiO)	Attack of electrolyte by FeO	$911 < T <$ 1376 K	$\Delta G^0 = -251\,480 - 18.1T + 10.187T \ln T$ ($\pm$210 J mol^{-1}) $T <$ 1184 K
		Atmosphere of purified Ar ($p_{O_2} < 10^{-13}$ bar)	Identical to Charrette and Flengas [72]	$\Delta G^0 = -286\,248 + 181.419T + 13.858T \ln T$ 1184 $< T <$ 1340 K
Sundman [73]	Compilation			$\Delta G^0 = 128.29T - 526\,107$ From Sjoden et al. [70] data

Table 11
Compilations and original works performed on the Gibbs energy of the $2Ni(s) + O_2(g) \leftrightarrow 2NiO$ equilibrium

Authors [Ref.]	Nature of the sample	Experimental technique	Chemical reference	ΔG_f^0 (J mol^{-1}) and comments
Markin [74]	Ni/NiO	E.m.f. (electrolyte ?)	Cu/Cu_2O [67]	$\Delta G^0 = -474\,047 + 173.6T$ $500 < T < 1000$ °C We do not understand how this result is obtained
Charrette and Flengas [72]	Ni/NiO or Fe/Fe_2O_3 powders	E.m.f. Ni, NiO/ZrO_2–0.1CaO/Fe, FeO or air /Pt cell under vacuum and closed avoid O_2 (Ar) contamination	Ni–NiO/air or Ni, NiO/Fe, FeO	$\Delta G^0 = -467\,302.6 + 169.8T$ (±210 J mol^{-1}) $911 < T < 1376$ Fe, FeO as reference: $\Delta G^0 = -526\,782 + 129.6T$ (±418 J mol^{-1}) $903 < T < 1540$ K
Saito [75]	Ni/NiO	E.m.f. (electrolyte ?) Ar purified	Fe/FeO Blumenthal and Whitemore [76]	$\Delta G^0 = -468\,357 + 170.2T$ $773 < T < 1273$ K
Berglund [77]	Ni/NiO (1/5) ratio to prevent sintering	E.m.f., ZrO_2–ThO_2 electrolyte Ar purified to carry H_2/H_2O p_{O_2} residual $= 2.9 \times 10^{-5}$ atm	H_2/H_2O [78]	$\Delta G^0 = -235\,071 + 86.2T$ $825 < T < 1675$ K
Comert and Pratt [79]	Ni/NiO (1/7)	E.m.f., Ni, NiO/ZrO_2–0.1CaO/air, Pt Ar purified, vacuum purged, Reversibility tests	Air	$\Delta G^0 = -232\,450 + 83.435T$ (±39 J mol^{-1}) $760 < T < 1275$ K
Neumann et al. [80]	Ni/NiO system	Compilation	Mah and Pankratz [81]	$\mathrm{Log} p_{O_2}$, bar $= 8.811 - 24400/T$ $Ni + 4/2O_2 \rightarrow NiO$ $1000 < T < 1713$ K

for O_2(g) when vaporizing oxygen rich oxides (evaporation coefficient). We discard for these reasons these data.

E.m.f. determinations of Une and Oguma [62] were run with an electrochemical cell referred directly to air in order to study the UO_2–Gd_2O_3 system. Other measurements cited in our work were systematically referred to Ni/NiO or Fe/FeO systems. Une and Oguma checked their electrode when redetermining the oxygen potential of these two systems: their chemical potential is lower than the retained ones in Appendix A by respectively 2660 and 24,500 J at 1273 K, and the slopes as a function of temperature differ. For $UO_{2+x}(2 + x > 2.02)$, their potentials are systematically higher than those retained to build our chart – by 1050–30,000 J – the larger the difference the closer the composition to stoichiometric UO_2. Two main features can be invoked to explains these trends: (i) the air electrode may have an accommodation coefficient (kinetic barrier in the $O_2 \rightarrow 2O^{2-}$ conversion), (ii) the uncertainty for compositions close to UO_2 may become significant due to calcination at 1023 K (the correction called here Ackermann's correction has to be applied). As these e.m.f. data do not overlap – within their uncertainty range – with our chart, we discard this work.

Thermogravimetric analysis of Une and Oguma [63] were run for UO_2 and UO_2–Gd_2O_3 systems under CO/CO_2 gas equilibration. The analyzed composition domain ranges from $O/U = 2.001$–2.07, with a reference to $UO_{2.001}$ under a fixed CO/CO_2 composition. The comparison in the 2.01–2.07 domain with our chart shows differences in the $-3500/+11\,100$J range at 1573 K, and in the $-8400/+5800$ J range at 1773 K. These data overlap with our chart, and consequently are retained for further optimization.

Thomas et al. [64] thermogravimetric determinations were performed mainly for compositions close to stoichiometric. UO_2 and with a 'quasi-stoichiometric' reference. As for references [34] and [35] we shall further analyze these data with those for stoichiometric and hypostoichiometric urania in a third paper.

Acknowledgements

The authors acknowledge Mr G. Sauzay and COGEMA for sponsoring this study, and Dr Paul Potter for help in the preparation of the final text.

Appendix A

Our choice of Gibbs energies for Ni/NiO and Fe/FeO diphasic systems used as references in e.m.f. studies. The sets of literature data are presented in Tables 10 and 11.

A.1. The Fe/FeO reference

The Gibbs energies for the reaction $2Fe(s) + O_2(g) = 2FeO(s)$ are presented in Fig. 20. Some differences appear between Richardson and Jeffes [65] and Kiukkola and Wagner [67] and others, their differences being larger than the published uncertainties. As we need only one reference to scale all e.m.f. studies performed on UO_{2+x}, we retain the data of Sundman [73] that have been already chosen for the optimization of the Fe–O system. This choice is based on the work of Sjoden et al. [71] that appears to be a compromise or mean value of earlier determinations. So,

$$\Delta_r G^0_T(\mathrm{Fe/FeO}) = -526\,107 + 128.29T(\pm 210\ \mathrm{J\,mol^{-1}})$$
$$790 < T < 1500\ \mathrm{K}.$$

A.2. The Ni/NiO reference

The original works on Ni/NiO are presented in Fig. 21, showing excellent agreement whatever the references: air/pt, H_2/H_2O, Cu/Cu_2O or Fe/FeO. The agreement

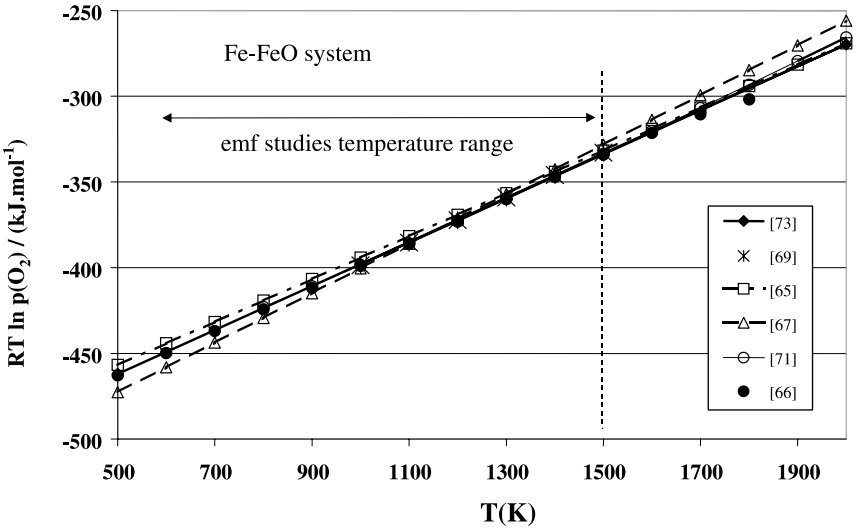

Fig. 20. Standard Gibbs energy of the reaction $2Fe(s) + O_2(g) => 2FeO(s)$.

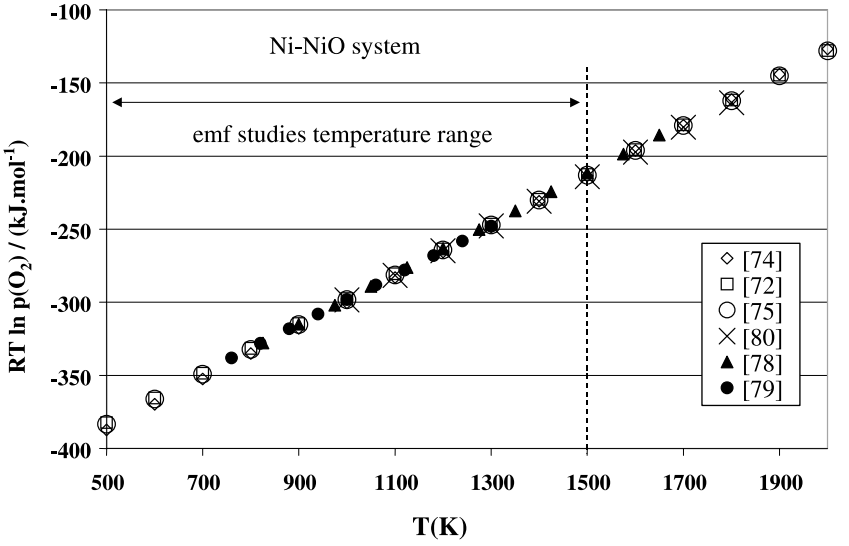

Fig. 21. Standard Gibbs energy of the reaction $2Ni(s) + O_2(g) => 2NiO(s)$.

with the Fe/FeO as reference justifies our choice for $\Delta G^0_T(\mathrm{Fe/FeO})$. Thus,

$$\Delta_r G^0_T(\mathrm{Ni/NiO}) = -467\,302.6 + 169.8T(\pm 210\ \mathrm{J\,mol^{-1}})$$
$$800 < T < 1500\ \mathrm{K}.$$

As a conclusion, all e.m.f. original data on UO_{2+x} have been re-scaled with these two consistent references, the uncertainties of which are very small.

References

[1] M.H. Rand, O. Kubaschewski, The Thermochemical Properties of Uranium Compounds, T. and A. Constable Ltd., Printers to the University of Edinburgh, 1963 (not quite the right format).
[2] B. Lindemer, T.M. Besmann, J. Nucl. Mater. 130 (1985) 473.
[3] Y.S. Kim, J. Nucl. Mater. 279 (2000) 173.
[4] K. Naito, N. Kamegashira, Adv. Nucl. Sci. Technol. 9 (1976) 99.
[5] P.Y. Chevalier, E. Fischer, J. Nucl. Mater. 257 (1998) 213.
[6] B. Jansson, Report TRITA-MAC-0234 April 1984, Royal Institute Technology, S10044 Stockholm 70, Sweden.
[7] F. Rossini, Experimental Thermochemistry, Interscience, New York, 1956, p. 308.
[8] O. Vittori, Méthodes électrochimiques, Polarographie, vol. P3, Les Techniques de l'Ingénieur (Ed.), 249 rue de Crimée, Paris cedex 9, France, 1988, p. 2135a, (www.techniques-ingenieur.fr).
[9] P.O. Perron, Report No. AECL-3072, 1968.
[10] T.M. Florence, Analytical Methods in the Nuclear Fuel Cycle, IAEA, Vienna, 1972, p. 45.
[11] E.A. Schaefer, M.R. Menke, J.O. Hibbits, Report No. GE-TM 66-4-9, 1966.
[12] B.D. Holt, J.E. Stoessel, Anal. Chem. 36 (1964) 1320.
[13] E.A. Schaefer, J.O. Hibbits, Anal. Chem. 42 (1969) 254.
[14] E.D. Lynch, J.H. Handwerk, C.L. Hoenig, J. Amer. Ceram. Soc. 43 (1960) 520.
[15] G.S. Petit, C.A. Kienberger, Anal. Chim. Acta 25 (1961) 579.
[16] E.H.P. Cordfunke, P. Aling, Trans. Faraday Soc. 61 (1965) 50.
[17] P. Gerdanian, M. Dodé, J. Chim. Phys. 62 (1965) 171.
[18] M.S. Rodriguez de Sastre, J. Philippot, C. Moreau, Report No. CEA-R 3218, France, 1967.
[19] R.J. Ackermann, A.T. Chang, J. Chem. Thermodyn. 5 (1973) 873.
[20] T. Fujino, H. Tagawa, T. Adachi, J. Nucl. Mater. 97 (1981) 93.
[21] P. Srirama Murti, R.B. Yadav, H.P. Nawada, et al., Thermochim. Acta 140 (1989) 299.
[22] R. Benz, G. Balog, B.H. Baca, High Temp. Sci. 2 (1970) 221.
[23] B. Sundman, J. Phase Equil. 12 (1991) 127.
[24] K. Kiukkola, Acta Chem. Scand. 16 (1962) 327.
[25] S. Aronson, J. Belle, J. Chem. Phys. 29 (1958) 151.
[26] T.L. Markin, R.J. Bones, UKAEA Report AERE-R4042 HL 62/2187 (C 3), UK, 1962.
[27] D.I. Marchidan, S. Matei, Rev. Roum. Chimie 17 (1972) 1487.
[28] D.I. Marchidan, S. Matei-Tanasescu, Rev. Roum. Chimie 18 (1973) 1681.
[29] D.I. Marchidan, S. Matei-Tanasescu, Rev. Roum. Chimie 19 (1974) 1435.
[30] D.I. Marchidan, S. Matei-Tanasescu, Rev. Roum. Chimie 20 (1975) 1365.
[31] D.I. Marchidan, S. Matei, Rev. Roum. Chimie 15 (1970) 1491.
[32] A. Nakamura, T. Fujino, J. Nucl. Mater. 149 (1987) 80.
[33] Y. Saito, J. Nucl. Mater. 51 (1974) 112.
[34] T.L. Markin, R.J. Bones, UKAEA Report AERE-R4178 HL62/5420 (C5) UK, 1962.
[35] V.G. Baranov, Yu.G. Godin, Atomic Energy 51 (1980) 228–230 (translation from Russian).
[36] A. Kotlar, P. Gerdanian, M. Dodé, J. Chim. Phys. 64 (1967) 1135.
[37] L.E.J. Roberts, A.J. Walter, J. Inorg. Nucl. Chem. 22 (1961) 213.
[38] K. Hagemark, M. Broli, J. Inorg. Nucl. Chem. 28 (1966) 2837.
[39] A. Kotlar, P. Gerdanian, M. Dodé, J. Chim. Phys. 64 (1967) 862.
[40] A.M. Anthony, R. Kiyoura, T. Sata, J. Nucl. Mater. 10 (1962) 8.
[41] T. Matsui, T. Tsuji, K. Naito, J. Nucl. Sci. Technol. 11 (1974) 216.
[42] A. Caneiro, J.P. Abriata, J. Nucl. Mater. 126 (1984) 255.
[43] P.E. Blackburn, J. Phys. Chem. 62 (1958) 897.
[44] E.D. Cater, Characterization of high temperature vapor and gases, Special Pub. 561/1, Nat. Institute Standards Technology, Gaithersburg MD 20889-0001, USA, 1979, p. 3.
[45] S. Banon, C. Chatillon, M. Allibert, High Temp. Sci. 15 (1982) 129.
[46] S. Dushman, Scientific Foundations of Vacuum Technique, John Wiley, New York, 1958 (Chapter 1).
[47] W.L. Winterbottom, J. Chem. Phys. 47 (1967) 3546.
[48] N.A. Gokcen, J. Phys. Chem. 69 (1965) 3538.
[49] J.W. Ward, R.J. Bivins, M.V. Fraser, J. Vac. Sci. Technol. 7 (1970) 206.
[50] P. Rocabois, C. Chatillon, C. Bernard, Rev. Int. Hautes Temp. Réfract. 28 (1993) 37.
[51] C. Younés, PhD at Université de Paris-Sud, Orsay, France, Order 14-3199, 26 June 1986.
[52] E.H.P. Cordfunke, R.J.M. Konings, Thermochemical Data for Reactor Materials and Fission Products, North Holland, Elsevier Science, Amsterdam, 1990.
[53] M.W. Chase Jr., NIST-JANAF Thermodynamical Tables, 4th Ed., 1998, J. Phys. Chem. Ref. Data., Monograph 9, Nat. Inst. Standards Technology, Gaithersburg, MD 20889-0001, USA.
[54] A. Gabriel, C. Chatillon, I. Ansara, High Temp. Sci. 23 (1987) 187.
[55] A. Caneiro, J. Nucl. Mater. 113 (1983) 260.
[56] C. Chatillon, P. Rocabois, C. Bernard, High Temp. High Press. 31 (1999) 413.
[57] D. Labroche, Thermodynamics of the U–O system, Original data of oxygen chemical potential in the UO_2–U_3O_8

composition range and presentation of the selected data set used to perform the optimization of the thermodynamic properties and phase diagrams, Report No. 2001/264, CEA/VRH, 26702 Pierrelatte, France, 2001.
[58] O. Dugne CEA/VALRHO, Pierrelatte, DFN/DTE/STMF/LMAC, BP 111, 26702 PIERRELATTE Cedex – France (EXCEL Format), e-mail: olivier.dugne@cea.fr.
[59] V.A. Kurepin, J. Nucl. Mater. 303 (2002) 65.
[60] P.Y. Chevalier, E. Fischer, B. Cheynet, J. Nucl. Mater. 303 (2002) 1.
[61] A.T. Chapman, R.E. Meadows, J. Amer. Ceram. Soc. 47 (1964) 614.
[62] K. Une, M. Oguma, J. Nucl. Mater. 110 (1982) 215.
[63] K. Une, M. Oguma, J. Nucl. Mater. 115 (1983) 84.
[64] C. Thomas, P. Gerdanian, M. Dodé, J. Chim. Phys. (Phys. Chim. Biol.) 65 (1968) 1349.
[65] F.D. Richardson, J.H.E. Jeffes, J. Iron Steel Inst. 160 (1948) 269.
[66] L.B. Pankratz, US Bureau Bull. 672 (1982).
[67] K. Kiukkola, C. Wagner, J. Electrochem. Soc. 104 (1957) 379.
[68] J.P. Coughlin, US Bur. Mines Bull. 542 (1954).
[69] K. Kiukkola, Acta. Chem. Scand. 16 (1962) 327.
[70] E. Takayama, N. Kimizuka, J Electrochem. Soc. 127 (1980) 970.
[71] O. Sjoden, S. Seetharaman, L.I. Staffansson, Met. Trans. B 17 (1986) 179.
[72] G.G. Charette, S.N. Flengas, J. Electrochem. Soc. 115 (1968) 796.
[73] B. Sundman, J. Phase Equil. 12 (1991) 127.
[74] T.L. Markin, R.J. Bones, Report AERE-R4042 HL 62/2187 (C3) UK, 1962.
[75] Y. Saito, J. Nucl. Mater. 51 (1974) 112.
[76] R.W. Blumenthal, D.H. Whitemore, J. Amer. Ceram. Soc. 44 (1961) 508.
[77] S. Berglund, Ber. Buns. Ges. 80 (1976) 862.
[78] S. Berglund, Rev. Int. Hautes Tempér. Réfract. 8 (1971) 111.
[79] H. Comert, J.N. Pratt, J Chem. Thermodyn. 16 (1984) 1145.
[80] J.P. Neumann, T. Zhong, Y.A. Chang, Bull. Alloy Phase Diag. 5 (1984) 141.
[81] A.D. Mah, L.B. Pankratz, US Bureau Mines Bull. 668 (1976).